UW Translational Imaging Biomarker and Therapeutic Development

Final Technical Report

Period Covered: 09/01/2014 through 08/31/2018

November 2018

Robert S Miyaoka
(Awarded to Satoshi Minoshima, MD, PhD)
University of Washington, Seattle, Washington

Team Members:
D. Scott Wilbur, PhD, Professor, UW Department of Radiation Oncology (Program Director)
Kenneth Krohn, PhD, Professor, UW Department of Radiology (Program Director)
Robert Miyaoka, PhD, Professor, UW Department of Radiology
Jeanne Link, PhD, Associate Professor, UW Department of Radiology
Donna Cross, PhD, Assistant Professor, UW Department of Radiology
James Fink, MD, Assistant Professor, UW Department of Radiology
John Grierson, PhD, Research Scientist, UW Department of Radiology
Steve Shoner, PhD, Research Scientist, UW Department of Radiology
Kevin Yagle, PhD, Research Scientist, UW Department of Radiology
Chun Yuan, PhD, Professor, UW Department of Radiology and Bioengineering
Jeffrey Schwartz, PhD, Associate Professor, UW Department of Radiation Oncology
Ethan Balkin, Ph.D., Postdoctoral Fellow, UW Department of Radiation Oncology
James Park, MD, FACS, Associate Professor, UW Department of Surgery
Brenda Sandmaier, MD, Professor, UW Medicine/Fred Hutchinson Cancer Research Center
John Pagel, MD, PhD, Associate Professor, UW Medicine/ Fred Hutchinson Cancer Research Center

PREPARED FOR THE US DEPARTMENT OF ENERGY
OFFICE OF SCIENCE FINANCIAL ASSISTANCE PROGRAM
UNDER CONTRACT NO. DE-SC0012445

Overall project Summary

Introduction: The development and validation of radiotracers is a critical step in the clinical translation of molecular imaging and radiotheranostics to support personalized medicine. The goal of this program was to support such efforts by an interdisciplinary team of investigators at the University of Washington (UW) and after the move of Dr. Minoshima at the University of Utah (U of U) and to provide opportunities for trainees to learn the spectrum of translational research in imaging biomarkers and therapeutic development. The integration of expertise of diverse research groups (radiochemists, imaging scientists, clinicians) is a common challenge in translational research. This funding opportunity will solidify ongoing efforts of integration at UW (and U of U) into a cohesive program that will train a new generation of investigators. This will, in turn, accelerate the translational potential of new radiotracers by rapid developments of proof-of-concept and first-in-man studies along with in vivo validations in a clinically relevant context. The proposed research mechanism is to use an interdisciplinary 'team' of expert investigators and trainees working on a specific project for 1 or 2 years along the timeline and milestones set by the Program Directors. UW (and U of U) provides outstanding research and clinical facilities and resources that can be accessed by investigators and programs. The Departments of Radiology and Radiation Oncology at UW (and Radiology at U of U) have been at the forefront of translational imaging and therapeutics research efforts in cancer, neurological disorders, and cardiovascular diseases. A brief summary of the goals of each project are provided below.

Project 1: Preclinical Evaluation of PET Imaging for use in the translation of targeted alpha therapy of blood-related cancers to clinical studies: Scott Wilbur, PhD (Project Leader); Brenda Sandmaier, MD; John Pagel, MD, PhD; Robert Miyaoka, PhD; Ethan Balkin, PhD (Senior Fellow, UW); Mazyar Shadman, MD (Senior Fellow, FHCRC); Corey Burden (Undergraduate, UW).

Project 1: Project Objectives

The overall objective of this research project was to conduct preclinical PET Imaging in mice and dogs using ^{124}I-labeled anti-CD45 antibody to obtain data that is instrumental to facilitate the design of clinical PET Imaging protocols to predict safety and therapeutic outcomes in patients with hematologic cancers after administration of an analogous ^{211}At-labeled anti-CD45 antibody. The preclinical studies involved PET Imaging of normal animals and mice with disseminated murine leukemia or human lymphoma, as well as dogs with lymphoma. Along with the imaging research project, a major secondary objective was to provide training of basic scientists and physicians in theory and methods relating to radiochemical, biomedical / imaging sciences, and clinical translation. The two specific objectives for the project were as follows:

Specific objective 1-1: Evaluate microPET imaging of ^{124}I---labeled anti-CD45 antibodies in normal mice and mice with disseminated human lymphoma or murine leukemia.

Specific objective 1-2: Evaluate ^{124}I-labeled anti-canine CD45 antibodies in PET studies of normal dogs and dogs with lymphoma.

Project 2: Hypoxia Imaging: Radiopharmaceuticals, Preclinical Studies, Mechanisms And Clinical trials: Kenneth Krohn, PhD (Project Leader); Jeanne Link, PhD; Steve Shoner, PhD; James Fink, MD; Jeffrey Schwartz, PhD; Robert Miyaoka, PhD; And Kevin Yagle, PhD

Project 2: Project Objectives

The Overall goal of this project was to evaluate radiotracers to assess tissue hypoxia, a critical micro-environmental factor affecting cancer treatment response. Our Previous research focused extensively on research and development of radiotracers to depict tissue hypoxia and clinical applications in various cancers. In This project, we will apply FMISO---PET To a critical public health problem, the response of patients to anti---angiogenesis therapies.

Specific Objective2-1: ^{18}F-FMISO---PET to study mechanisms of response and resistance to anti-angiogenic therapy in animal models.

Specific Objective 2-2: Evaluate hypoxia as a result of anti-VEGF therapy in glioblastoma patients.

Specific Objective 2-3: Characterize ^{64}Cu(ATSM) and the role of copper in tumor biology.

Project 3: Diagnostic Applications Of Radiolabeled Biologics In Solid Tumors: Satoshi Minoshima, MD, PhD (Project Leader); John Grierson, PhD; James Park, MD; Donna Cross, PhD, Robert Miyaoka, PhD; Chun Yuan, PhD; Geoffrey Baird, MD, PhD (Laboratory Medicine); Jonathan Sham (Resident, Surgery); Gabriel Fine, MD, PhD (Resident, Radiology)

Project 3: Project Objectives:

The overall objective of this project was to advance imaging and future theranostic applications of biologics, namely antibodies and aptamers, that are being developed in our laboratory and to conduct preclinical PET imaging of ^{89}Zr labeled anti-Glypican-3 antibody (αGPC3) in the mouse model of hepatocellular carcinoma (HCC) and liver cirrhosis and ^{89}Zr or ^{18}F labeled aptamer, Epidermal Growth Factor Receptor (EGFR) SOMAmers in animal xenograft models of EGFR overexpressing tumors. Through these projects, we will produce data that are necessary for further translational efforts to human studies and also provide training opportunities for physicians and basic scientists. The four specific objectives were as follows:

Specific Objective 3-1: Validate detection accuracy of ^{89}Zr labeled αGPC3 antibody PET imaging targeting implanted HCC in mice that have developed clinically relevant liver cirrhosis and compare its diagnostic accuracy to standard MRI.

Specific Objective 3-2: Conduct ^{89}Zr labeling of humanized aGPC3 antibodies and perform proof-of-concept microPET imaging in preparation for translational applications in humans.

Specific Objective 3-3: Establish labeling strategies for ^{89}Zr of ^{18}F EGFR SOMAmers.

Specific Objective 3-4: Evaluate ADME characteristics of radiolabeled EGFR SOMAmers in mouse models with microPET imaging.

We hypothesize that 1) radiolabeled anti αGPC3 antibody PET will be able to detect small HCC in cirrhotic liver more accurately than standard MRI; 2) humanized antibody will be able to achieve biodistribution comparable to our previous murine antibodies; and 3) radiolabeled aptamer will accumulate in target tumors at the level detectable by PET imaging.

We note that Dr. Minoshima, PI Project 3 and overall PI, moved to the University of Utah during the funding period of this grant. This led to a redirection of the aims of Project 3 as described in the Project 3 final report below. Also with his move, Dr. Miyaoka took over as overall PI of the grant.

Individual project summaries are provided below.

Final Report for Project 1 of the DOE-funded Research Project entitled "UW Translational Imaging Biomarker and Therapeutic Development"

Project 1: Preclinical Evaluation of PET Imaging for Use in the Translation of Targeted Alpha Therapy of Blood-Related Cancers to Clinical Studies

Project Leaders: D. Scott Wilbur (UW) and Brenda Sandmaier (FHCRC)
Other contributors to this project (experiments and/or writing): Ethan R. Balkin, Donald Hamlin, Aimee Kenoyer, A. Lake Wooten, Maryline (Ferrier) Kerlin

---

1. Introduction

The overall objective of this research project was to conduct preclinical PET imaging in mice and dogs using ^{124}I-labeled anti-CD45 antibodies to obtain data that will help design clinical PET imaging protocols to predict safety and therapeutic outcomes in patients with hematologic cancers treated with ^{211}At-labeled anti-CD45 antibody. The preclinical studies were to include PET imaging of normal mice and mice with disseminated murine lymphoma or leukemia, as well as normal dogs and pet dogs with lymphoma. Along with the imaging research project, a secondary objective was to provide training of basic scientists and physicians in theory and methods relating to radiochemical, biomedical/imaging sciences, and clinical translation. The three specific objectives for the project were:

Specific Objective 1: Evaluate ^{124}I-labeled anti-CD45 antibodies in microPET imaging of normal athymic mice and athymic mice with implanted human lymphoma or leukemia.

Specific Objective 2: Evaluate ^{124}I-labeled anti-canine CD45 antibodies in PET/CT studies of normal dogs and dogs with lymphoma.

Specific Objective 3: Provide training opportunities for undergraduate, graduate, postdoctoral fellows and medical residents in conducting the research study.

Our preclinical results suggest that ^{211}At-labeled anti-CD45 monoclonal antibody (MAb) can be effective for hematopoietic stem cell transplantation (HSCT), and that it might be used in the treatment of malignant or non-malignant diseases in patients. After considerable preclinical studies, it has been shown that ^{211}At-labeled anti-CD45 MAb used with HSCT improved the median survival of leukemic mice in a dose-dependent manner with minimal toxicity, suggesting that this approach may be a promising new therapeutic option for AML.(1) Canine models have also been studied, in which ^{211}At-labeled anti-CD45 MAb for myeloablation prior to HSCT as part of the regimen for treating cancers of the hematopoietic system have been evaluated. Such therapy could reduce or eliminate the dose of total body irradiation (TBI) that is required for conditioning the marrow for HSCT. All these efforts led to our obtaining two NIH Program Project grants (PO1) to evaluate ^{211}At-labeled anti-CD45 MAb-B10 in clinical studies, one to the National Cancer Institute (NCI) and another to National Heart Lung and Blood Institute (NHLBI), using ^{211}At-labeled anti-CD45 MAb for marrow conditioning in trial participants. Based on the preclinical study results, an IND was filed by the Fred Hutchinson Cancer Research Center (FHCRC) and Food and Drug Administration (FDA) approval was obtained to conduct a Phase I clinical trial for treatment of blood-related cancers. That clinical trial has begun.

The investigation was conducted to determine if PET imaging could be used to obtain tissue dose estimates for patients undergoing the ^{211}At-labeled anti-CD45 treatment of blood-related cancers. At the onset of the studies, it was unclear which data from the imaging would provide the most useful information for predicting toxicity and treatment outcome. However, *we hypothesized that evaluation of ratios of tissue concentrations obtained in PET imaging might be*

predictive of the toxicity and therapy outcomes. Our intention was to show that PET imaging of blood-related cancers in animal models (both mice and dogs) provided tissue concentrations (liver, kidney, lung, spleen, lymph node, bone, etc.) that were significantly different in normal vs. cancer-bearing mice, such that the information could be used for predicting toxicities and therapy outcomes.

PET imaging was performed by using the radiopharmaceutical labeled with a positron emitting radionuclide, ^{124}I, which was chosen for its similarity of chemistry with ^{211}At and for its properties useful for PET imaging. Our studies demonstrated that ^{124}I can be reacted with the same anti-CD45 MAb-B10 conjugate as used with ^{211}At, and that substitution of radioiodine does not decrease target cell binding. Although ^{124}I has a low abundance of positron emissions (23%), a high (weighted) average energy of positron emission ($E_{B+,avg}$ = 0.82 MeV), and a large number of high-energy gamma-ray emissions, this isotope has the potential to be used in quantitative PET imaging (2-4) with MAbs and their fragments (5-9) because its half-life ($t_{1/2}$ = 4.176 d) is long enough to obtain data over the biological half-lives of these cancer-targeting agents. Furthermore, in dual-label studies in mice (10) and dogs (11), we have shown that MAbs conjugated with the isothiocyanato-phenethylurido-*closo*-decaborate(2-) [designated B10-NCS] can be labeled with both radioiodine- (^{123,125,131}I-) and ^{211}At-labeled anti-CD45 and that co-injected mixtures have essentially the same tissue biodistributions. Other PET radionuclides cannot be used as the MAb-B10 conjugate would have to be replaced with a different labeling moiety, which would alter the tissue biodistribution. This would be problematic in estimating the tissue doses and toxicity.

2. Methods

Radiolabeling

[1] Approximately 3.5 mCi of ^{124}I was obtained from 3D Imaging (Maumelle, Arkansas). A preliminary labeling experiment was conducted to test reaction conditions. In the experiment, 100 µg of BC8-B10 conjugate was reacted with 110 µCi ^{124}I and 10 µg of chloramine-T as oxidant in phosphate buffered saline (PBS), pH 6.8 at room temperature. The labeling reaction was allowed to progress for 1 minute prior to quenching with sodium metabisulfite, at which point the content of the reaction vessel were loaded onto a PD-10 column which had been pre-conditioned with phosphate buffered saline (PBS) for purification by size exclusion chromatography. The column was eluted with nine 0.5 mL fractions of PBS. Selecting the fractions with the highest counts (highest yielding fractions, in these conditions Fractions 6 & 7), had 91.0 µCi of product providing a labeling efficiency of 82.3%. The HPLC chromatogram of the collected product displayed a single product peak with an area of 99.8% showing no shoulder or tailing characteristics.

[2] An anti-human CD45 MAb conjugate, BC8-B10, ^{124}I-labeling experiment for a mouse imaging/biodistribution study used the following procedure: A 6.6 µL aliquot of [^{124}I]NaI, 1.5 mCi, was added to a vial containing 25 µL of 0.5 M sodium phosphate. That mixture was added a 1008 µL PBS solution containing 5.0 mg/mL of BC8-B10 (5040 µg), followed by addition of 104 µL of a 1 mg/mL chloramine-T in deionized water. The reaction was allowed to proceed for 1 min at room temperature, then 104 µL of a 1 mg/mL aqueous solution of sodium metabisulfite was added to quench it. After purification by size-exclusion chromatography (PD-10), 743 µCi (55.6%) of ^{124}I-BC8-B10.

[3] A second BC8-B10 ^{124}I-labeling experiment for a mouse imaging/biodistribution study was conducted in a similar manner. In that experiment 1500 µg of BC8-B10 was reacted with 2.6 mCi [^{124}I]NaI and 37 µg of chloramine-T to yield 1.90 mCi (77.6%) of ^{124}I-BC8-B10.

[4] An anti-canine CD45 MAb conjugate, CA12.10C12-B10, ^{124}I-labeling experiment was conducted in a similar manner. In that experiment 2000 µg of BC8-B10 was reacted with 6.9 mCi [^{124}I]NaI and 50 µg of chloramine-T to yield 5.90 mCi (92.6%) of ^{124}I-CA12.10C12-B10.

Description of imaging procedure

Mice. On the day of the study, the mice were transferred to University of Washington Medical Center (UWMC). The labeled product was injected, and the typical acquisition time for PET was 30 min at early time points and 1 h for later time points. Imaging was performed, on 2 out of 5 mice, at 1, 2, 4, and 24 hours post-injection. After final imaging time point, all five animals were sacrificed pursuant to the UW Office of Animal Welfare and a post-necropsy biodistribution study was conducted via gamma counting of the collected tissues.

Dogs. Dog imaging studies required transporting the dog from FHCRC to Harborview Medical Center (HMC). It was also required that the radiolabeled MAb conjugate, ^{124}I-CA12.10C12-B10 be transported from UWMC to HMC. The labeled product was injected. The typical time points for PET/CT imaging were 1, 2, 4, 24 h post-injection of the radiolabeled ^{124}I-CA12.10C12-B10, and the typical acquisition time for PET was 30 min at early time points and 1 h for later time points. After final imaging time point, the dog was transported to FHRC, euthanized according to regulation and a post-necropsy biodistribution study was conducted via gamma counting of the collected tissues.

Camera calibration using a phantom

A ~250 µL aliquot of ^{124}I of stock vial for use in calibration and phantom measurements. The ^{124}I (229 µCi) was then diluted in 50 mL of normal saline and loaded into a capped syringe, which was then used as a phantom for PET. Cross calibration of the dose calibrator, gamma well counter, and PET instrument was then performed by the generation of conversion factors, such that a value obtained in any of the three detectors could be easily compared to or converted to the scale of any other detector. In this case, it was found that the conversion factor for the PET scanner to the dose calibrator was 1.0427 µCi/mL and that the conversion factor between the well counter and the dose calibrator was 3.233×10^{-6} µCi/CPM. This exercise was repeated prior to each animal study to account for variability in the activity per volume of the injectate.

PET/CT Imaging

Equipment for mouse imaging studies: Imaging was conducted using the *Inveon microPET* (Siemens Preclinical Solutions, Knoxville, TN) instrument in the UW Animal Bioimaging Center at UWMC. This scanner includes an adjacent coaxial small animal CT scanner (Siemens Preclinical) for accurate PET/CT fusion. Operation of the microPET instrument and image reconstructions were conducted by Dr. Robert Miyaoka and his staff in the imaging facility, but quantitative image analysis was performed by our group.

Equipment for dog imaging studies: Imaging was conducted on a state-of-the-art Philips human time-of-flight (TOF) PET/CT scanner with sub-millimeter CT imaging and time of flight PET technology at UW Harborview Medical Center. Operation of the TOF PET instrument and data collection were conducted by Barbara Lewellen, of Dr. Robert Miyaoka's staff.

Imaging Analysis Methods

Specific data collection and workup of collected images including: (1) calculations of regions of interest (ROIs) for heart, liver, kidney, lung, spleen, femur, and lymph node bed; (2) evaluation of average values with standard deviations for the ROI's among the groups of mice at each time point.

Data in the results presented

All data in this report are given as an average value of data obtained in these studies and their standard deviations. The biodistribution values are obtained from the average of the data measured on the 5 mice, and for the dog the average value is calculated from 3 samples from the same tissue in one dog. The imaging values are taken from 2 mice and their average and standard deviations are presented. For the dog imaging, a single dog was analyzed so the values are the ones from this analysis and the standard deviation from software of these values are given.

3. Project Objectives

***Specific Objective 1:* Evaluate ^{124}I-labeled anti-CD45 MAbs in microPET imaging of normal athymic mice and athymic mice with disseminated human lymphoma or murine leukemia.**

Goal: *The goal of this specific objective is to determine if the differences in tissue concentrations, and ratios of concentrations in regions of interest, obtained from ^{124}I microPET imaging studies in normal mice and mice with disseminated murine leukemia and lymphoma are large enough to be useful when evaluating safety and efficacy of the injected ^{211}At-labeled radiopharmaceutical.*

Mouse Study 1: Pilot Imaging Study

This study is focused on data obtained from ^{124}I microPET imaging using ^{124}I-BC8-B10 in normal nod/SCID mice. The goal of this study was to gain a foundation and understanding of biodistribution and imaging data on normal mice. Nod-SCID mice (female, 25 g, 12 weeks old, n=5) were used in this study. The mice were housed in the Fred Hutchinson Cancer Research Center (FHCRC) animal resource center until the time of the study, then they were transferred to University of Washington (UW) for the imaging study. It should be noted that the mice were not disease-bearing and had not been implanted with xenografts to be used as a model of diseased animals. The ^{124}I-BC8-B10 was diluted with PBS and BC8-B10 was added to bring the injectate to the desired specific activity. Ten doses were prepared, 1 dose for each study mouse and 5 standards. After preparation, the doses were delivered to the imaging facility for injection. At the time of the study, each animal was injected with 210 μg of ^{124}I-labeled BC8-B10 at a dose of 50 μCi and then anesthetized for evaluation by microPET imaging (2/5 mice) and tissue harvest biodistribution (all 5 mice). Imaging procedure was followed as described above in the experimental section.

In this section Figures 1 and 2 present data obtained by ex vivo tissues gamma counting biodistribution and in vivo PET imaging data, respectively. First, Figure 1 provides graphed data obtained in a biodistribution of the radiopharmaceutical in the mice 24 hours post injection.

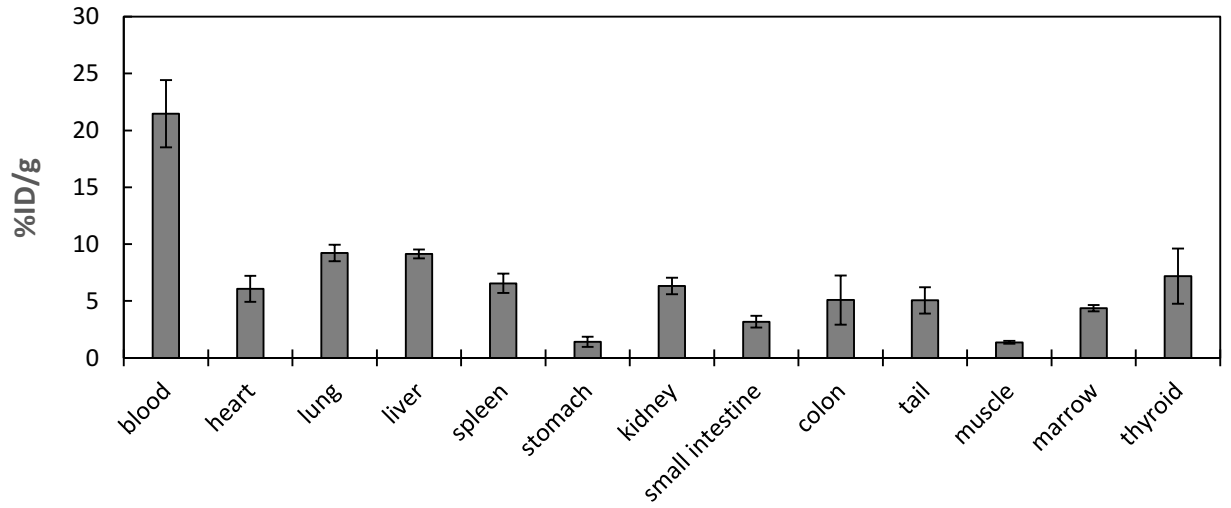

Figure 1. Tissue concentrations of ^{124}I-BC8-B10 obtained by gamma counting of ex vivo tissues.

Figure 2 shows the in vivo concentration of the radiolabeled compound in the mice at 2, 4, and 24 hours post injection. The data at 24 hours can be compared to ex vivo gamma counted tissues to determine the effectiveness of the PET imaging compared to gamma counting.

The highest concentration of the radiolabeled compound at 24 hours post injection was in the blood, followed by concentrations in organs that participate to the metabolism and excretion of the radiolabeled antibody, liver, spleen, kidney and colon. Unfortunately, high percentages (> 5%) are also found in heart, lung, marrow and thyroid.

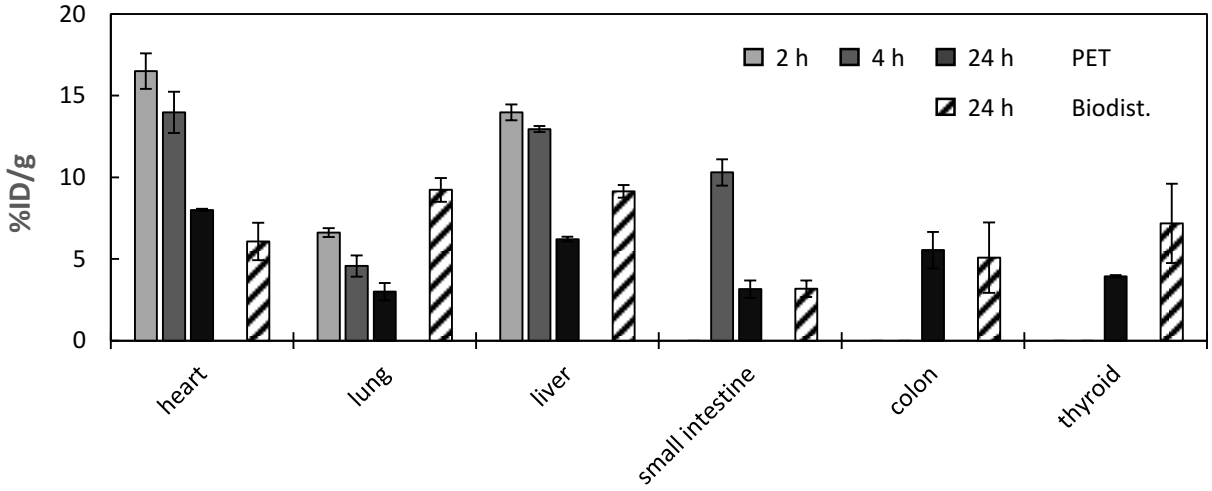

Figure 2. Tissue concentrations of [^{124}I]-BC8-B10 at 2, 4 and 24 h post injection, as obtained by quantitative analysis of in vivo PET images (in shades of grey/black) and data obtained by PET and by post-necropsy gamma counting of tissues at ~24 h post injection (white with black pattern).

Figure 2 clearly shows that over time, the concentration of radiolabeled antibody decreases. When the data at 24 hours from the PET imaging and the biodistribution (ex vivo gamma counting) is compared, it appears that the imaging data is over estimating for the heart, is similar or within the error for small intestine and colon, but under estimated for lung, liver and thyroid. The error associated with gamma counting for thyroid tissue is quite large, perhaps from not being able to obtain thyroid tissue, but the data obtained by in vivo PET imaging appears to be more consistent.

Mouse Study 2: Biodistribution of human Burkitt lymphoma using [^{124}I]-BC8-B10

This study was focused on data obtained from ^{124}I microPET imaging using ^{124}I-BC8-B10 in nod/SCID mice with and without lymphoma (Ramos disseminated model). The goal of the study was to determine if the differences in tissue concentrations, and ratios of concentrations in regions of interest are large enough to be useful when evaluating safety and efficacy of the injected ^{211}At-labeled radiopharmaceutical in potential future studies. The BC8 MAb targets the extracellular portion of the transmembrane human CD45 receptors of hematopoietic cells. Normal and diseased (Ramos xenograft, mice injected with 1x10^6 Ramos i.v. 14 days before study) mice (5 each) were injected with a radiolabeled MAb-B10 conjugate for evaluation by microPET imaging. The imaging procedure followed was as described above in the experimental section.

Figures 3, 4 and 5 present concentration (injected dose /g) data obtained from gamma counting of mice tissues and from in vivo PET imaging, and provide a comparison of that data at 24 hours post injection. Figure 3 shows tissue concentrations of the radiopharmaceutical in mice at 24 hours post injection in normal mice and mice injected with Ramos cells (14 days before treatment). Figure 4 shows tissue concentrations of the radiopharmaceutical at 2, 4, and 24 hours post injection for the two groups of mice. Figure 5 compares the tissue concentrations obtained from ex vivo gamma counted tissues with the PET image data.

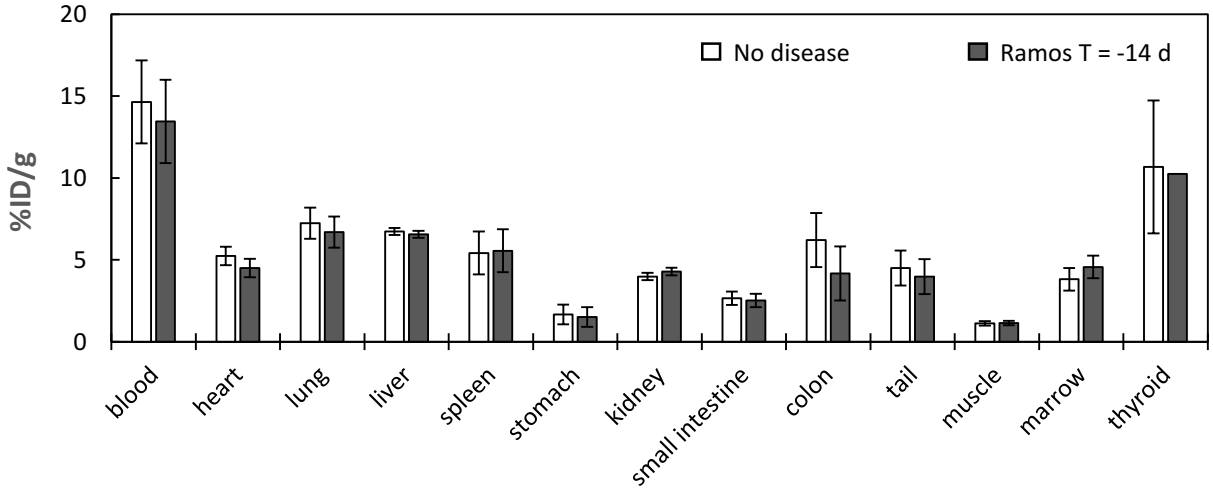

Figure 3. Tissue concentrations of ^{124}I-BC8-B10 obtained by gamma counting of ex vivo tissues.

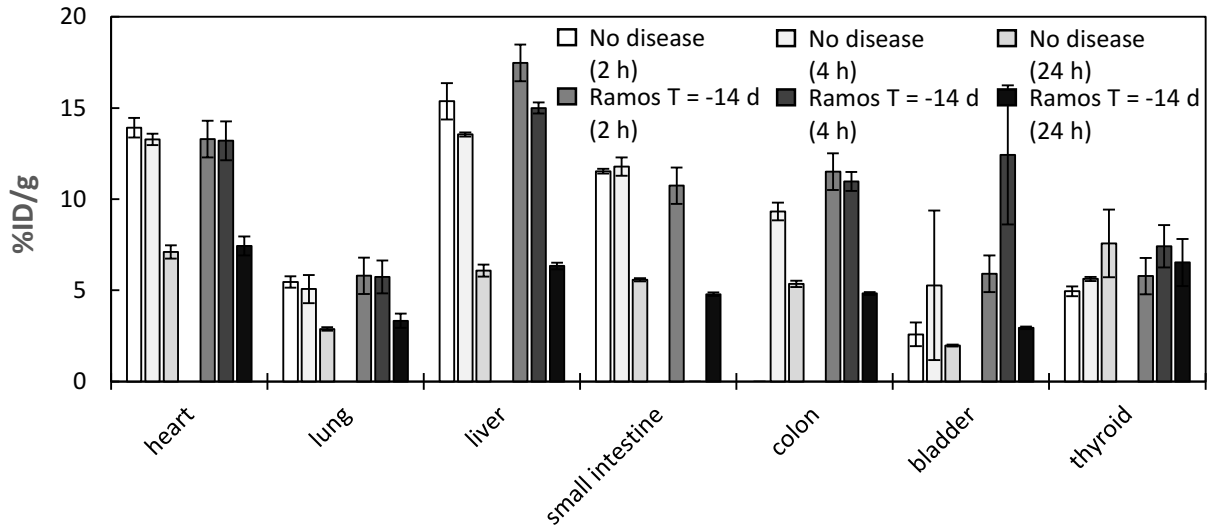

Figure 4. Tissue concentrations of [^{124}I]-BC8-B10, measured by quantitative analysis of in vivo PET images acquired at 2,4,24 h post-injection.

This comparison can be used to evaluate the accuracy of the PET imaging data relative to gamma counting for both groups of mice. Unfortunately, the biodistribution data shows that the differences in tissue concentration between the normal mice and mice injected with Ramos cells are within the standard error bars.

Figure 4 data shows that the concentration of the radiolabeled antibody decreases in most tissues with time. The exception is the bladder, where a high concentration at 4 hours could relate to the time of excretion and metabolism of the drug. This organ seems to have different concentrations if the mice are disease bearers or not, but the concentrations can vary greatly due to bladder emptying. Another exception seems to be the thyroid which has a difference pharmacokinetic behavior than the other organs in normal mice and Ramos bearing mice. Again, this difference may be due to differences in metabolism in the mice and not due to disease presence.

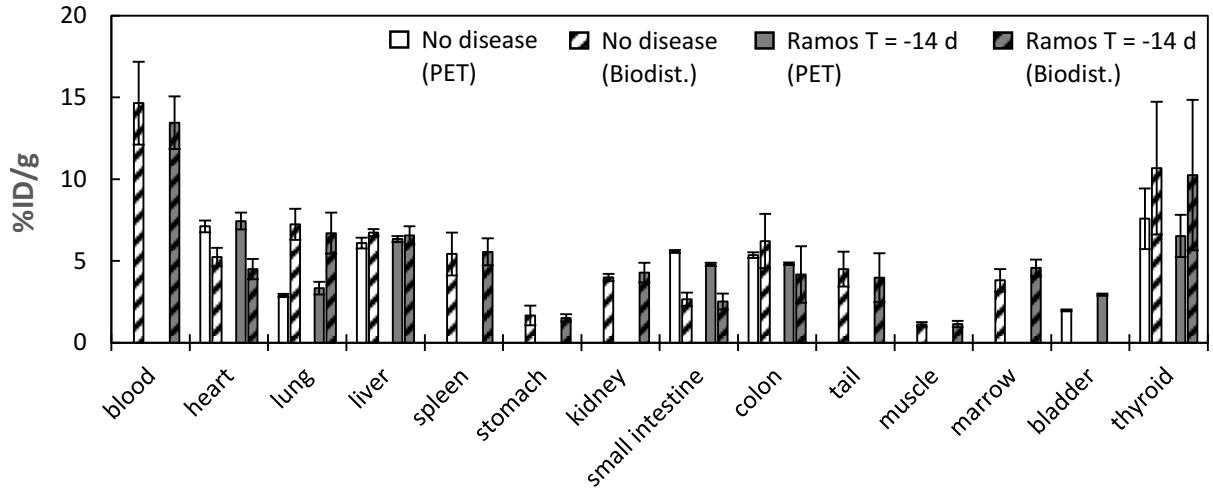

Figure 5. Comparison of tissue concentrations of ^{124}I-BC8-B10, obtained by PET at ~24 h and by post-necropsy gamma counting of tissues.

Figure 5 shows a comparison of the tissue concentrations obtained from PET imaging and from tissue counting. Even after 24 hours, it can be observed that a high concentration remains in the blood and in the thyroid. Concentrations > 5% injected dose / gram are found in liver and spleen, but kidney and colon concentrations are less than 5% ID/g. However, a high concentration is found in heart and lung, while the marrow is below 5%. When comparing PET data and biodistribution it appears that PET imaging is over estimating the heart and small intestine concentrations, while the concentrations in colon and liver are similar or within the standard error. In contrast, it appears that PET imaging underestimates the lung and thyroid concentrations. As previously found, the variance in thyroid concentrations obtained with gamma counting is quite large, while the data obtained by in vivo PET imaging could be within the standard error.

Mouse Study 3: Biodistribution of AML using [^{124}I]30F11-B10

This study was focused on tissue concentration data obtained from ^{124}I microPET imaging using a murine anti-CD4 MAb, ^{124}I-30F11-B10 in SJL/J mice with and without murine AML. Again, the goal of this study was to determine if the differences in tissue concentrations in regions of interest are large enough to be useful when evaluating safety and efficacy of the injected ^{211}At-labeled radiopharmaceutical in potential future studies. The 30F11 MAb targets the extracellular portion of the transmembrane murine CD45 receptors of murine hematopoietic cells. Normal and diseased (SJL cell xenograft, mice injected with $1x10^5$ SJL cells i.v.) mice (5 each) were injected with a ^{124}I-labeled MAb for evaluation by microPET imaging.

Figures 6 and 7 graphically present tissue concentrations (ID/g) obtained by ex vivo gamma counting and in vivo PET imaging. Figure 8 compares the 24-hour post injection data obtained by the two methods. Figure 6 shows the tissue concentrations of the radiopharmaceutical in normal mice and mice bearing murine AML cells (14 days before treatment) at 24 hours post injection. Figure 7 shows the tissue concentrations of the radiopharmaceutical in the mice at 3.5, 5.5, and 24 hours post injection. In Figure 8 the 24-hour data can be compared to determine the accuracy of the PET imaging compared to gamma counting.

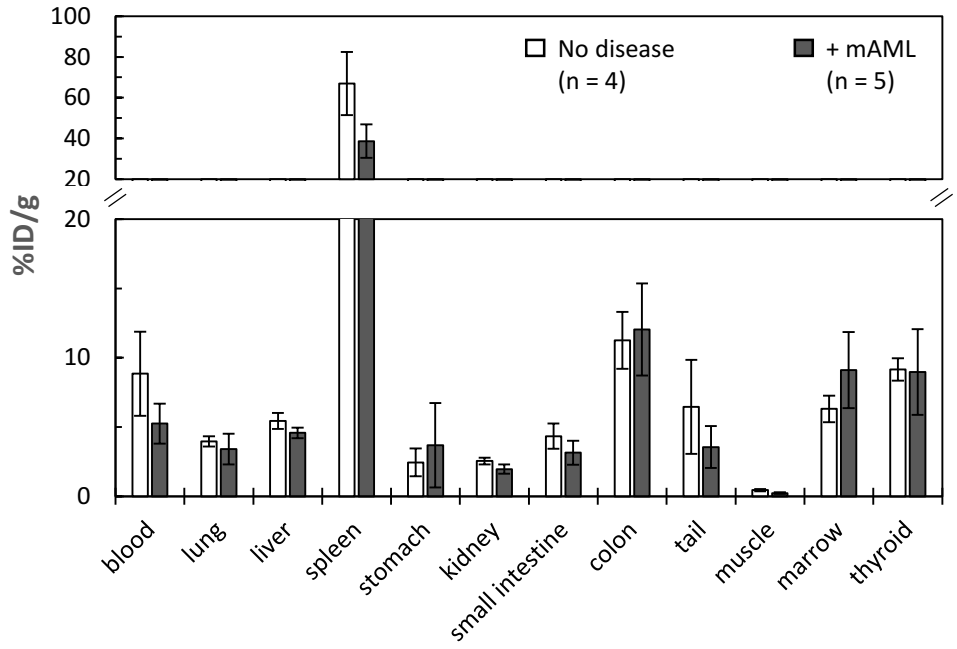

Figure 6. Tissue concentrations of ^{124}I-30F11-B10 obtained by gamma counting of ex vivo tissues.

It can be noted that in Figure 6 there are no major differences between the concentrations of ^{124}I-labeled MAb in the two groups of mice. However, it appears that normal mice have higher concentrations of radiolabeled antibody in the blood and spleen, while having lower concentrations in the marrow than the mice with AML.

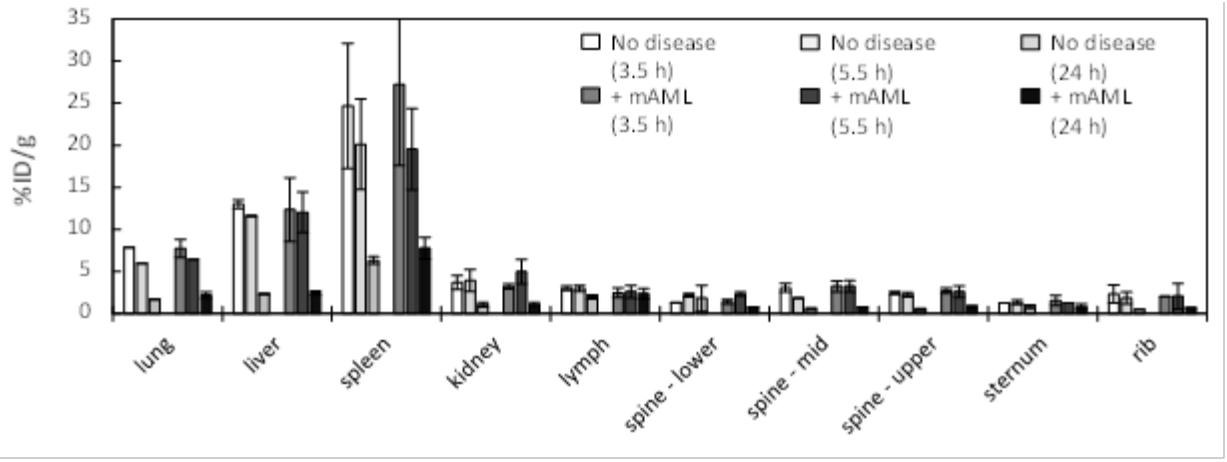

Figure 7. Tissue concentrations of [^{124}I]-30F11-B10, obtained by quantitative analysis of in vivo PET images.

Figure 7, similar to that observed in previous studies, shows that the concentrations of labeled antibody decrease in the organs over time. While this is expected, it seems noteworthy to point out that the concentrations in liver and spleen (> 10%) appear elevated at 1.5, 3.5 and 5.5 hours

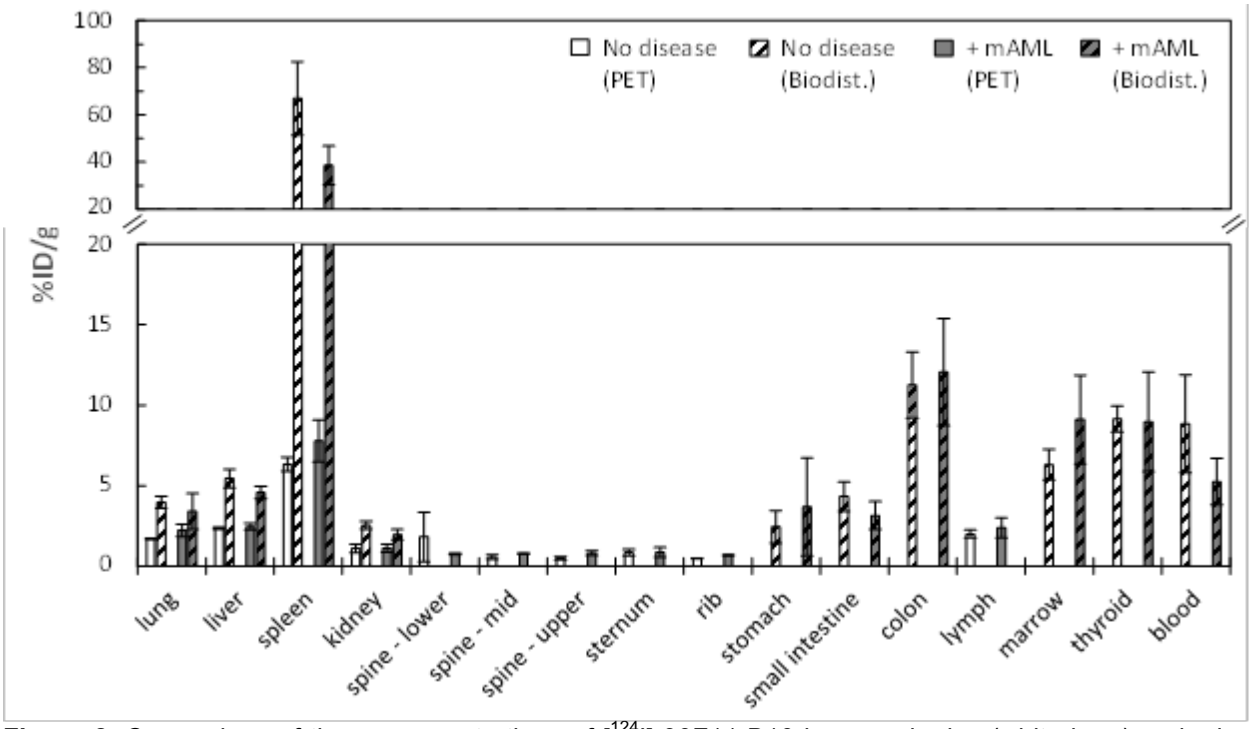

Figure 8. Comparison of tissue concentrations of [^{124}I]-30F11-B10 in normal mice (white bars) and mice bearing mAML (grey bars), obtained by PET imaging (denoted by full color bars) and by post-necropsy gamma counting of tissues (denoted by pattern bars) at ~24 h post injection.

post injection, but drop dramatically at 24 hours to < 3% and < 8%. Also, it can be noted that the concentrations in the lymph nodes appear to stay constant in both groups over the 24 hours observation time. Figure 8 appears to indicate that all data from PET in vivo imaging underestimate the concentrations obtained by gamma counting.

<u>Specific Objective 2:</u> Evaluate ^{124}I-labeled anti-canine CD45 MAbs in PET/CT studies of normal dogs

Goal: *The goal of this specific objective is to determine if the differences in tissue concentrations, and ratios of concentrations in regions of interest, obtained from ^{124}I PET/CT imaging in normal dogs.*

PET/CT imaging was conducted on 2 normal dogs. No pet dogs with lymphoma were referred to the protocol so no data was obtained for comparison with the normal dogs. The canine MAb, CA12.10C12 was used in this portion of the study as it specifically targets the extracellular portion of the transmembrane CD45 receptor of hematopoietic cells in the canine model. While no PET dogs were referred, the study design included PET/CT imaging of pet dogs with lymphoma. In that arm of the study, the lymphoma dogs would be administered ^{124}I-labeled CA12.10C12-B10 five days prior to the ^{211}At-labeled radiopharmaceutical. This period of time was chosen as it is long enough to allow the radiolabeled MAb to clear from the blood and tissues prior to injection of the ^{211}At-labeled MAb-B10. Also, this is a short enough time period to not illicit dog-anti-mouse antibodies (DAMA) production prior to the ^{211}At-labeled MAb-B10 injection. The methods for the imaging/biodistributions studies were described above in the experimental section. Data are presented for two normal dog studies.

Figure 9 shows the ^{124}I-CA12.10C12-B10 blood clearance obtained blood samples at predetermined times in both dogs. It can be noted that the blood clearance was very similar for the two dogs.

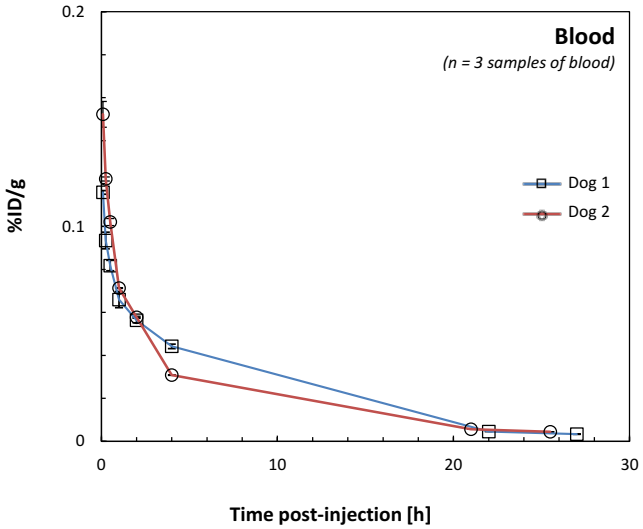

Figure 9. Time-activity curve for blood clearance of ^{124}I-CA12.10C12-B10 MAb measured by gamma counting of blood samples from the two dogs.

Figure 10 shows a comparison of tissue concentrations of ^{124}I-CA12.10C12-B10 in tissues after necropsy of the two healthy dogs at 24 hours post injection.

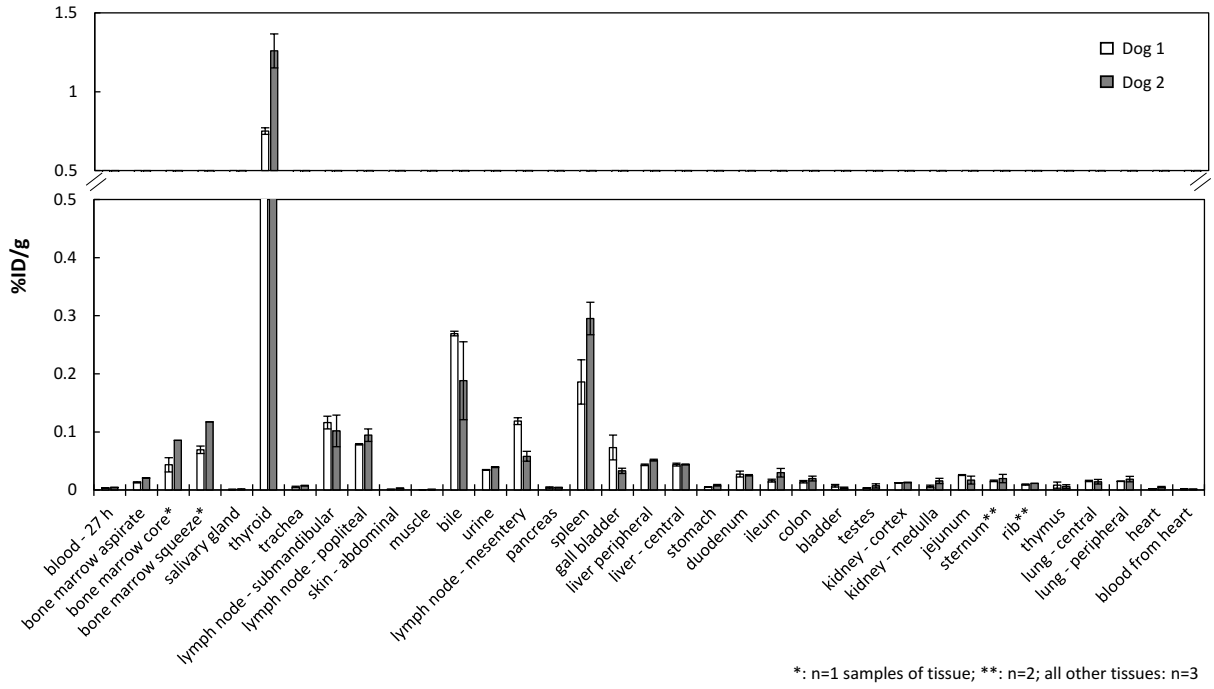

Figure 10. Biodistribution of ^{124}I-CA12.10C12-B10 MAb measured by gamma counting of tissues from necropsy for the two dogs.

Figure 10 shows no major difference in tissue concentrations between the two healthy dogs. At 24 hours post injection, a high concentration of ^{124}I is present in the thyroid, and smaller quantities of activity were observed in the bile, spleen, bone marrow and lymph nodes. Differences between the dog tissue concentrations were noted. Specifically, Dog #2 had higher concentrations in bone marrow, thyroid, and spleen, but lower concentrations in bile and some lymph nodes. It seems likely that the metabolism of the two dogs is different.

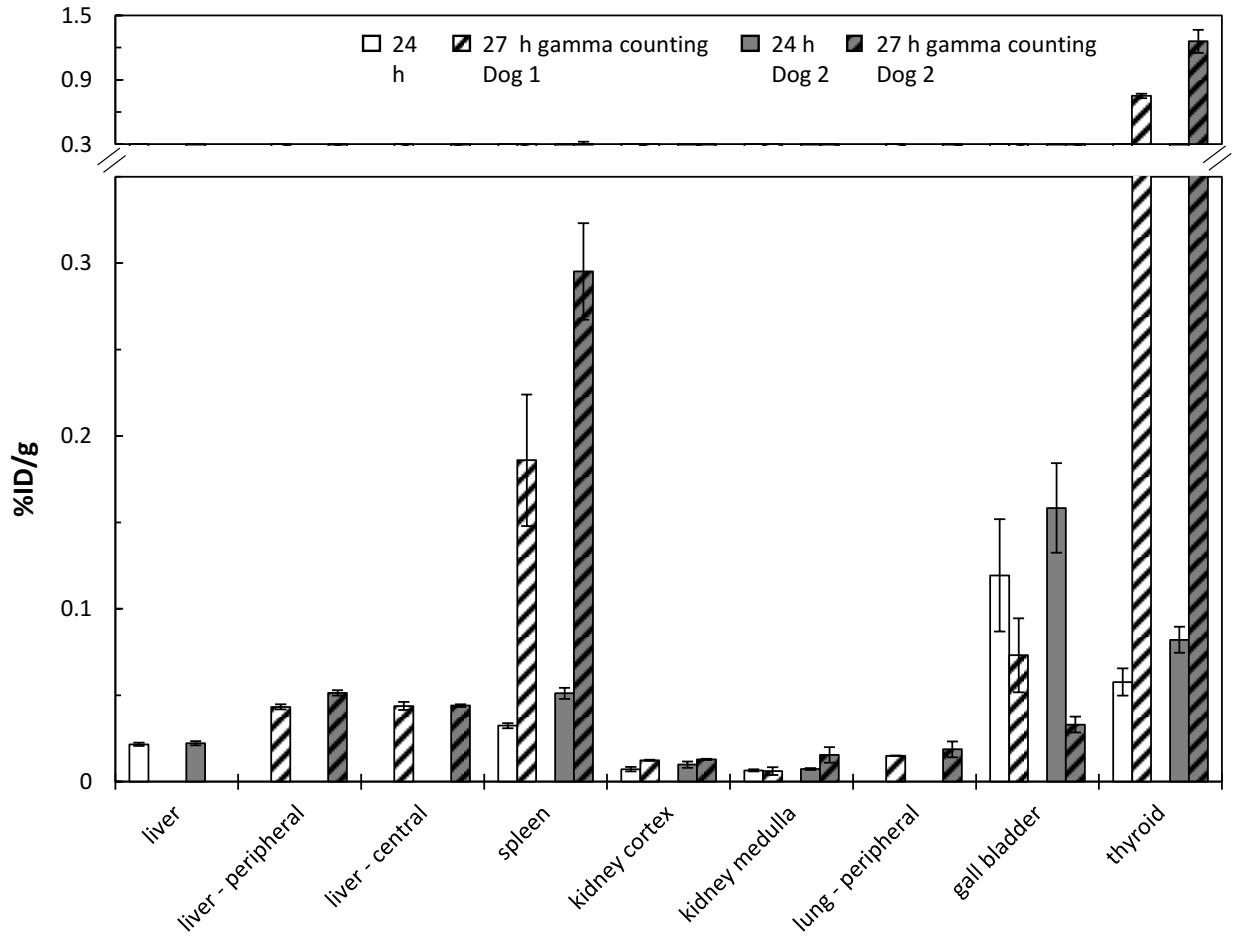

Figure 11. Comparison of tissue concentrations of ^{124}I-CA12.10C12-B10 MAb in dog #1 (white bars) and dog #2 (grey bars) measured by PET at ~24 h (plain color) post injection. That data can be contrasted with the tissue concentrations obtained by post-necropsy gamma counting of tissues (bars with black pattern on colored bars).

From the data plotted in Figure 11 it appears that the in vivo PET imaging is underestimating the concentrations in liver, spleen and thyroid, but overestimating the concentration in the gall bladder.

CONCLUDING COMMENTS

This investigation was conducted to determine if PET/CT imaging of the same MAb-B10 conjugate that was used to deliver ^{211}At in blood-borne cancer treatment protocols might be used to predict toxicity and efficacy. Unfortunately, the large discrepancies found between the concentrations estimated by PET imaging and by tissue counting after necropsy makes this approach questionable. If there are overestimations and underestimations of the actual quantity of activity in tissues, there could be large errors in dose estimated in those tissues. Thus, use of PET/CT for dosimetry may not provide accurate enough dose estimates to predict toxicity and efficacy in this application. We have provided a table below (Table 1) that shows the overestimation and underestimation discrepancies found by PET imaging of mice and dogs at ~24 hours post injection.

Table 1. Comparison of in vivo PET imaging data with ex vivo gamma counting data at ~ 24 hours for all studies in this report. Legend:

Organs	Mouse study 1	Mouse study 2	Mouse study 3	Dog study 1	Dog study 2
Heart	↑	↑	-	-	-
Lung	↓	↓	↓	-	-
Liver	↓	✓	↓	↓	↓
Small intestine	✓	↑	-	-	-
Colon	✓	✓	-	-	-
Thyroid	↓	↓ / ✓	↓	↓	↓
Spleen	-	-	↓	↓	↓
Kidney	-	-	↓	✓	✓
Gall Bladder	-	-	-	↑	↑

↑: PET imaging has a higher value than gamma counting; ✓: PET imaging has a similar value than gamma counting; ↓: PET imaging has a lower value than gamma counting; -: no measured at least with one of the 2 methods.

Specific Objective 3. **Offer training opportunities for undergraduate, graduate, postdoctoral fellows and medical residents in conducting the research study.**

Goal: *The goal of this specific objective is to engage undergraduate students, graduate students, Postdoctoral Fellows and Residents in radiopharmaceutical preparation, PET imaging process and interpretation of results from the imaging studies.*

Training was an integral part of this project. Researchers from UW and FHCRC participating in this research project were actively involved in training of students and postdoctoral fellows and participated regularly in "brainstorming" meetings to discuss the research progress of the three projects. Trainees involved in this work included: Ethan R. Balkin (former postdoc), Mazyar Shadman (former postdoc), A. Lake Wooten (former postdoc), Corey Burden (former undergraduate), Vlad Vlasenko (former undergraduate).

Literature Citations

1. Orozco JJ, Bäck T, Kenoyer A, Balkin ER, Hamlin DK, Wilbur DS, et al. Anti-CD45 radioimmunotherapy using ^{211}At with bone marrow transplantation prolongs survival in a disseminated murine leukemia model. Blood. 2013;121(18):3759-67.
2. Pentlow KS, Graham MC, Lambrecht RM, Cheung N-KV, Larson SM. Quantitative imaging of 1·124 using positron emission tomography with applications to radioimmunodiagnosis and radioimmunotherapy. Medical Physics. 1991;18(3):357-66.
3. Pentlow KS, Graham MC, Lambrecht RM, Daghighian F, Bacharach SL, Bendriem B, et al. Quantitative Imaging of Iodine-124 with PET. J Nucl Med. 1996;37:1557-62.
4. Koehler L, Gagnon K, McQuarrie S, Wuest F. Iodine-124: a promising positron emitter for organic PET chemistry. Molecules. 2010;15(4):2686-718.
5. Wilson CB, Snook DE, Dhokia B, Taylor CVJ, Watson IA, Lammertsma AA, et al. Quantitative measurement of monoclonal antibody distribution and blood flow using positron emission tomography and ^{124}Iodine in patients with breast cancer. Int J Cancer. 1991;47:344-7.
6. Bakir MA, Eccles SA, Babich JW, Aftab N, Styles JM, Dean CJ, et al. c-erbB2 Protein Overexpression in Breast Cancer as a Target for PET Using Iodine-124-Labeled Monoclonal Antibodies. J Nucl Med. 1992;33:2154-60.
7. Lee FT, O'Keefe GJ, Gan HK, Mountain AJ, Jones GR, Saunder TH, et al. Immuno-PET quantitation of de2-7 epidermal growth factor receptor expression in glioma using ^{124}I-IMP-R4-labeled antibody ch806. J Nucl Med. 2010;51(6):967-72.
8. Carrasquillo JA, Pandit-Taskar N, O'Donoghue JA, Humm JL, Zanzonico P, Smith-Jones PM, et al. ^{124}I-huA33 antibody PET of colorectal cancer. J Nucl Med. 2011;52(8):1173-80.
9. Schwartz J, Humm JL, Divgi CR, Larson SM, O'Donoghue JA. Bone marrow dosimetry using ^{124}I-PET. J Nucl Med. 2012;53(4):615-21.
10. Wilbur DS, Thakar MS, Hamlin DK, Santos EB, Chyan MK, Nakamae H, et al. Reagents for Astatination of Biomolecules. 4. Comparison of Maleimido-closo-Decaborate(2-) and meta-[211At]Astatobenzoate Conjugates for labeling anti-CD45 Antibodies with [^{211}At]Astatine. Bioconjugate Chem. 2009;20:1983-91.
11. Wilbur DS, Chyan MK, Nakamae H, Chen Y, Hamlin DK, Santos EB, et al. Reagents for astatination of biomolecules. 6. An intact antibody conjugated with a maleimido-closo-decaborate(2-) reagent via sulfhydryl groups had considerably higher kidney concentrations than the same antibody conjugated with an isothiocyanato-closo-decaborate(2-) reagent via lysine amines. Bioconjug Chem. 2012;23(3):409-20.

Final Scientific/Technical Report

Project 2: Project leader is Kenneth A Krohn, PhD

3. Executive Summary

This project addressed two important issues related to how tissues respond to very low levels of oxygen (Study 1) and a controversial new imaging agent for measuring regional low levels of oxygen, called hypoxia (Study 2). Oxygen is essential for mammals, including humans, to survive. When cells do not have an adequate supply of oxygen, they react in either of two ways. If the oxygen supply is cut off abruptly, tissues die over the period of a few hours. This happens in a stroke or myocardial infarction. However, it the oxygen supply is reduced slowly, an adaptive change occurs. The latter process was our focus. When tumors grow larger than a few tenths of an inch in diameter, they begin to exceed the ability of oxygen to diffuse from their blood supply and reach nearby cells. Specifically, the cells closest to a blood vessel get enough oxygen but the oxygen level is quickly consumed and so cells more than a millimeter away don't get essential oxygen. The growth of a tumor is slow enough that the cell's DNA reprograms itself to make proteins that help the hypoxic cells survive. Sometimes this involves angiogenesis, the process of sprouting new blood vessels to penetrate the growing tumor mass, sometimes adapting metabolism of glucose to gain more energy from each sugar molecule, and frequently by making enzymes that help cancer cells to escape their initial location and metastasize. Thus, finding and controlling these hypoxic cells is critically important in treating cancer and to diagnosing other biomedical conditions.

Our first study involved imaging the amount of hypoxia in cancer patients who are being treated with Avastin®, a drug that is intended to treat cancer angiogenesis but that also has the potential to increase hypoxia by causing the new blood vessels to collapse. Our second study involved testing a putative hypoxia imaging biomarker that might be useful for imaging cancer and neurodegenerative diseases. Our goal was to better define its mechanism for localization and its specificity for hypoxia versus other factors that only correlate with hypoxia but involve different biochemistry. We have made good progress on this aim but ended up with many new questions as we gained some answers for our original questions.

4. Comparison of original goals and actual accomplishments

Study 1— ^{18}FMISO-PET to study mechanisms of response to anti-angiogenic therapy.

This study included animal and human studies, with the proviso that if we found a physician trainee interested in the study, we would do the human studies rather than the animal studies. This was attractive because the anti-vascular therapies using antibodies have been optimized for patients rather than rodents. The goal of the cancer therapy is to use anti-vascular drugs, both small molecules and antibodies, to effectively starve the tumor of nutrients essential for their survival, including oxygen. We found such a trainee, Melinda Peck, MD, and she did several human imaging studies that are reported in the next section. In view of this, we did not carry out the animal studies.

Study 2— ^{64}Cu(ATSM) and the role of copper in tumor biology.

^{64}Cu(ATSM) was originally proposed as an imaging agent for hypoxia due to its increased uptake in hypoxic versus normoxic tissue in cells and in isolated hearts (Fujibayshi 1997). This was thought to be due to the low redox potential of ^{64}Cu(ATSM) compared to other thiosemicarbazone complexes (*e.g.,* the structurally related ^{64}Cu(PTSM), which is recognized as a blood flow imaging agent). This mechanism of reduction was expected to cause retention of radioactive Cu from ATSM but not from PTSM at low oxygen levels. Recent literature reports have challenged that mechanism and our objective was to test the mechanism of uptake and retention of different copper-based compounds labeled with ^{64}Cu made with our cyclotron. We used a simple *in vitro* cell model, the human red blood cell, because it does not have mitochondria, which complicate the mechanism. This project consumed the majority of our group effort for Project 2. While we did not resolve the many issues related to copper biology, we have made significant contributions that are summarized in the next section and will be reported in a manuscript in the next few months.

5. Summary of project activities

Study 1— ^{18}FMISO-PET to study mechanisms of response to anti-angiogenic therapy.

A functioning vascular network is essential for growth and survival of solid tumors (Hanahan 1996; 2011). Blocking new blood vessel formation (angiogenesis) in tumors is being exploited to stop or slow tumor growth (Folkman 1971) and thus starve the tumor. Two different approaches to *antiangiogenic* therapy have been developed. The first to receive FDA approval was bevacizumab, a monoclonal antibody to human vascular endothelial growth factor (hVEGF). The second uses small molecule pan-tyrosine kinase inhibitors (TKIs) to target VEGF receptors with drugs such as sorafenib. Multiple clinical trials have shown early remarkable radiographic response by gadolinium-enhanced T1 MR imaging and improved time to progression in tumors but patients eventually failed as tumors adapted and regrew. This has led to a disappointing improvement in overall survival. The role of antiangiogenesis therapy is hotly debated, with a growing realization that inhibition of the new vasculature growth may alter the natural history of cancer cells by increasing invasion and distant spread more than by starving the tumor cells. There is debate about why or even whether halting anti-VEGF therapy leads to rebound growth. These issues have clinical implications for development of effective therapy and they warrant detailed studies in animals as well as investigation in patients.

This aim described both animal and human studies, with the proviso that if we found a physician trainee interested in the study, we would do the human studies rather than the animal studies because the anti-angiogenic therapies have been optimized for patients rather than small animals. We found such a fellow, Melinda Peck, MD, and she did several human studies exemplified in Figure 1. The imaging studies used [^{18}F]FMISO, a thoroughly validated PET imaging agent (Krohn 2008). Imaging was done for four patients with studies at baseline and after two courses of bevacizumab.

Figure 1. T1Gd-MRI, FLAIR and ^{18}FMISO-PET scans of a patient with a recurrent glioma. The top row is before and the bottom row is after treatment with an anti-vascular antibody. The hypoxic region is black with a hole in the center indicating dead cells.

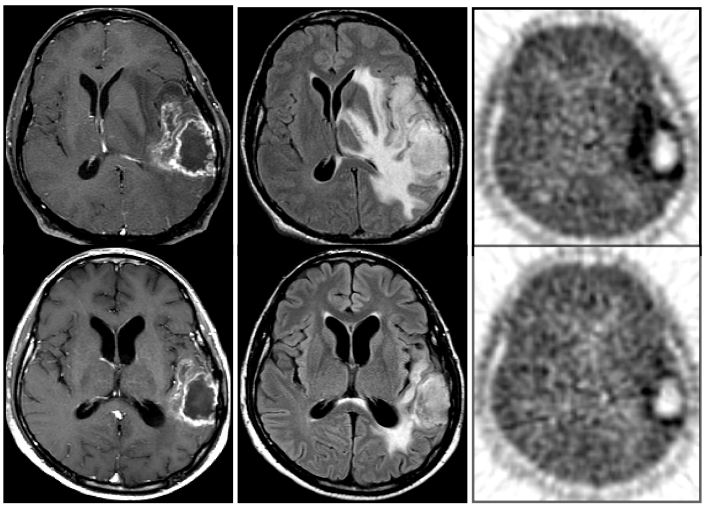

The hypoxic volume in this patient was reduced from 76 cc to 23 cc after therapy. Thus hypoxia imaging showed an early and positive response to anti-vascular therapy.

Unfortunately this patient died of the brain tumor within six months and before he returned for a follow-up scan. We expect the later scan would show florid hypoxia and provide evidence

about why this treatment fails to prolong survival. As part of this study, we completed four patient studies before Dr. Peck left UW. These studies have not been published because the number of patients is much too small and we need at least one additional follow up study. Two other groups have published on this same subject (Barajas 2016; Yamaguchi 2016) because of its importance. However, as part of her training, Dr. Peck participated in two review articles that are listed here,

Publications:

Fink JR, Muzi M, Peck M, Krohn KA. Multimodality Brain Tumor Imaging: MR Imaging, PET, and PET/MR Imaging. J Nucl Med. 2015 Oct;56(10):1554-61. doi: 10.2967/jnumed.113.131516. Epub 2015 Aug 20. Review. PubMed PMID: 26294301; PubMed Central PMCID: PMC4592410.

Peck M, Pollack HA, Friesen A, Muzi M, Shoner SC, Shankland EG, Fink JR, Armstrong JO, Link JM, Krohn KA. Applications of PET imaging with the proliferation marker [^{18}F]-FLT. Q J Nucl Med Mol Imaging. 2015 Mar;59(1):95-104. Epub 2015 Mar 4. Review. PubMed PMID: 25737423; PubMed Central PMCID: PMC4415691.

Study 2— ^{64}Cu(ATSM) and the role of copper in tumor biology

^{64}Cu(ATSM) was originally proposed as an imaging agent for hypoxia due to its increased uptake in hypoxic versus normoxic cultured cells and in isolated hearts (Fujibayshi 1997). This was thought to be due to the low redox potential of ^{64}Cu(ATSM) compared to other thiosemicarbazone complexes (*e.g.,* the blood flow agent ^{64}Cu(PTSM)). This allowed reduction and retention of Cu at low PO_2. Recent experiments challenged this mechanism by showing that both Cu-acetate and $CuCl_2$ had the same biodistribution kinetics as the Cu-thiosemicarbazone coordination compounds (Burgman 2005). All of these copper compounds involve Cu^{+2} but copper also has a Cu^{+1} oxidation state that is thought to be important in its retention.

Despite these inconsistent laboratory findings, numerous clinical studies have demonstrated significant potential of ^{64}Cu-ATSM as a predictive biomarker. Increased tumor uptake in cancer is well established and has correlated with poor patient outcome, whether or not it is a specific imaging biomarker for hypoxia (Dehdashti 2008). Elevated copper associated with cancer in both serum and tumor tissue is widely appreciated and copper levels have been shown to correlate with cancer stage, progression and regression. Furthermore, recent investigations of ^{64}Cu-ATSM deposition in neurodegenerative diseases including Alzheimer's, Parkinson's, and ALS, have suggested that it is a marker for oxidative stress and is correlated to cognitive and motor function decline. Thus, the mechanism question is important and far reaching.

METHODS: Our research involved a simple study of the mechanism of uptake and retention of ^{64}Cu-ATSM in cells *in vitro*. Numerous mechanistic studies have implicated the mitochondrial electron transport chain modified as a consequence of hypoxia as the dominant factor in uptake and retention. However, mechanistic studies are complicated by the role endogenous copper and cuproenzymes play in inflammation, neurotransmitter production, wound healing, angiogenesis, metabolism, and combating reactive oxygen species, ROS. Free copper ion is highly redox reactive and is toxic when in excess, potentially damaging proteins, lipids, and DNA. Thus homeostatic mechanisms have evolved to tightly control copper-binding interactions. We

reasoned that the red blood cell would provide a good model for investigating Cu-chelate deposition because erythrocytes lack a mitochondrial compartment and components of the ETC, but they still uses critical aspects of eukaryotic copper biology, including the central role of Cu/Zn-SOD1 and its copper-dependent role in ameliorating oxidative damage to the red cell. Endogenous copper levels in erythrocytes are estimated at approximately 10^6 atoms per cell. *In vivo,* the copper ion circulates in plasma as Cu(II), with > 75% bound to ceruloplasmin, a multi-copper binding ferroxidase. Unlike eukaryotic cells, which use a transmembrane protein, CTR1, for import of the trace co-factor, uptake of Cu(II) into the red blood cell is thought to occur via the anion exchanger band-3 protein.

With this background, we reasoned that the red blood cell would be the ideal model for our studies. In order to gain consistency in comparison experiments, all studies used blood from a single donor drawn fresh for each day's experiments. All comparisons reported here are for side-by-side comparisons with the same day's red cells. Our experiments were designed to modify copper biology within red cells in two different ways. (1) NADH-treated: NADH was added to a concentration of 40 µM in the bulk solution and incubated 15 min at 37 °C before adding the desired ^{64}Cu chelate. (2) Cu-depleted: NH_4 tetrathiomolybdate (TTM) is a high affinity chelator developed to treat copper excess in Wilson's disease. TMM was added to the fresh red blood cells at a final concentration of 10 µg/mL in order to deplete them of copper. Treated cells were incubated at 37°C on a slow rocker for 1 hr then washed 3x with PBS to remove TTM and diluted back to the original volume in PBS +10 µM glucose.

RESULTS: Adding either ^{64}Cu-PTSM or ^{64}Cu-ATSM to normal red cells gave much lower uptake than for ^{64}Cu-acetate (Fig 2). ^{64}Cu-PTSM uptake was ~ 4x higher than ^{64}Cu-ATSM, consistent with their difference in redox potentials modulating cellular deposition. While it is largely thought that Cu-PTSM can be reduced by ubiquitous glutathione, some evidence suggests that elevated NAD(P)H levels or associated reductases are responsible for conversion of Cu-ATSM to the less stable anionic complex. Our results for ^{64}Cu-ATSM added to NADH-treated cells support a mechanism that is not influenced by NADH/NAD+ redox balance. A 400-fold increase in NADH showed no significant increase relative to side-by-side untreated red cells (Fig 3).

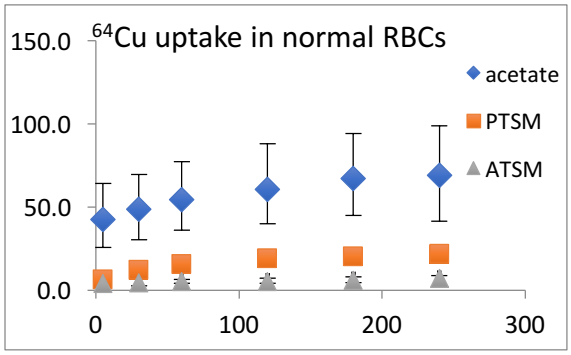

Fig 2. Percentage uptake of ^{64}Cu chelates fresh red cells. Time in minutes.

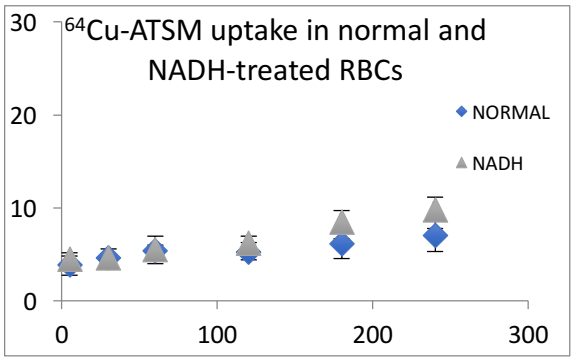

Fig 3. Uptake of ^{64}Cu-ATSM in normal *vs.* in normal NADH-added red cells.

Addition of ^{64}Cu-PTSM to NADH-treated red cells did not alter accumulation compared to untreated cells (data not shown but similar to Fig 3 except plateaued at ~20%). This was expected as the higher redox potential of Cu-PTSM should reduce indiscriminately in the cell. It is not yet

clear whether addition of NADH increased turnover of the ^{64}Cu-PTSM chelate and uptake was attenuated by an efflux mechanism for the copper drug or via endogenous copper efflux mechanisms. However, uptake curves of ^{64}Cu-PTSM for NADH-treated versus normal red cells were remarkably similar at all time-points.

Adding ^{64}Cu-acetate to NADH-treated cells gave a much different result, a significant increase in uptake, demonstrating that high levels of NADH result in twice as much copper accumulation (Fig 4). TMM-induced copper deficiency in the red cells significantly increased uptake for both ATSM and PTSM. TTM should deplete copper from more concentrated but lower affinity cellular components, leaving any available trace metal bound to high-affinity cuproproteins. This is consistent with a nearly quantitative deposition of copper tracer from ^{64}Cu-PTSM (Fig 5). ^{64}Cu-ATSM in TTM-treated cells also gave a 4-5-fold increase in uptake relative to untreated cells; it plateaued at just below 30%. This result is consistent with a ligand dissociation rate dependent on availability of a high affinity and thermodynamically favored cuproprotein acceptor for released ^{64}Cu(I) from the anionic complex. However, the suppression of ^{64}Cu-ATSM deposition in TTM-treated red cells was much larger than for ^{64}Cu-PTSM, consistent with µM to nM levels of copper chaperones and cuproenzymes versus mM levels of glutathione. Octanol extraction of the cell pellet after ^{64}Cu-PTSM detected no intracellular intact chelate at any time, consistent with the lower stability of the anionic PTSM complex and rapid transfer of tracer to the endogenous pool after reduction. ^{64}Cu-ATSM, however, showed detectable and reproducible levels of intracellular chelate for both untreated and NADH-treated cells at initial times but decreasing over time. There was no significant difference in levels of intact chelate for untreated and NADH-treated cells, consistent with reduction being zero order in NADH. However, in TTM treated cells, there was no measureable intact ^{64}Cu-ATSM at any times.

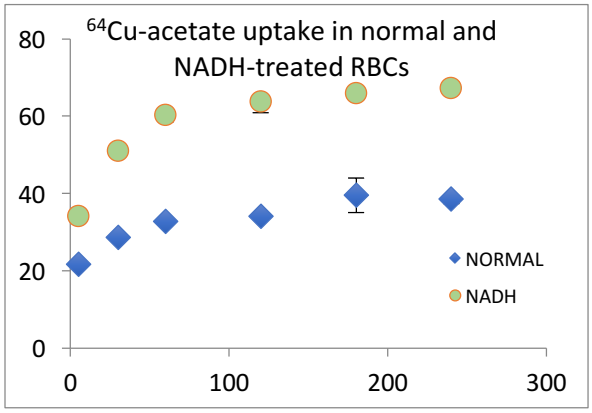

Fig 4. ^{64}Cu-acetate is much higher in NADH-treated red cells.

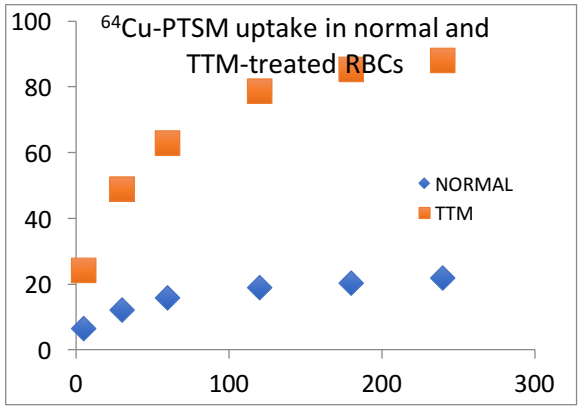

Fig 5. ^{64}Cu-PTSM uptake approaches 100% uptake in copper-depleted RBCs.

Our evidence suggests that the deposition of Cu-ATSM may be rate-limited by the availability of high-affinity and thermodynamically-favorable binding to specific cuproproteins. Deposition of ^{64}Cu-ATSM has been shown to correlate with hypoxia, oxidative stress, and mutant Cu,Zn-SOD1 pathology, all of which are modulated by relative levels of intracellular high affinity copper chaperone. CSS is capable of diverting the ^{64}Cu trace co-factor away from mitochondrial respiration in times of cellular oxidative stress, correlating Cu-ATSM deposition to hypoxia, oxidative stress, and a higher NADH redox status. We conclude from our studies that it is

inappropriate to call Cu-ATSM a hypoxia-imaging agent because it does not interact directly with oxygen. However, it is clearly a negative predictor of the outcome for cancer and probably other pathologies brought on by oxidative stress. In addition, our studies reconcile some physical biochemical arguments regarding the fate of Cu(I) ions after intracellular reduction and dissociation.

There are important questions that arise from our studies, mostly related to the role small thiol molecules such as glutathione versus tightly-controlled cuproprotein biochemistry. This has numerous implications with respect to cancer therapies involving thiol redox-related therapies such as cisplatin and anthracyclines, and extending to radiometal decorporation therapy related to dirty bombs.

Publications:

A full publication for peer review of our ATSM studies will be submitted in a few weeks. An abstract of our initial finding was presented at SNMMI in 2017 and a pdf of the poster is attached as an appendix item. (Copy of poster on the following page.)

Shirley A. Rene, Steven C. Shoner, Kevin J. Yagle, Kenneth A. Krohn. Copper ATSM/PTSM Mechanism in Cells without Mitochondria. Poster presentation at the annual meeting of Society of Nuclear Medicine and Molecular Imaging, Denver, June 2017. J Nucl Med 58(Suppl 2):905.

References

Barajas RF, Krohn KA, Link JM, Hawkins RA, Clarke JL, Pampaloni MH, Cha S. (2016) Glioma FMISO PET/MR Imaging Concurrent with Antiangiogenic Therapy: Molecular Imaging as a Clinical Tool in the Burgeoning Era of Personalized Medicine. *Biomedicines* **4**(4). pii: E24. doi: 10.3390/biomedicines4040024. PubMed PMID: 28536391; PubMed Central PMCID: PMC5344267.

Burgman P, O'Donoghue JA, Lewis JS, Welch MJ, Humm JL, Ling CC. (2005) Cell line-dependent differences in uptake and retention of the hypoxia-selective nuclear imaging agent Cu-ATSM. *Nucl Med Biol*. **32**:623–630.

Dehdashti F, Grigsby PW, Lewis JS, Laforest R, Siegel BA, Welch MJ. (2008) Assessing tumor hypoxia in cervical cancer by PET with ^{60}Cu-labeled diacetyl-bis(N^4-methyl-thiosemicarbazone). *J Nucl Med* **49**(2):201-5. doi: 10.2967/jnumed.107.048520. Epub 2008 Jan 16. PubMed PMID: 18199612.

Folkman J. (1971) Tumor angiogenesis: therapeutic implications. *N Engl J Med* **285**(21):1182-1186.

Fujibayshi Y, Taniuchi H, Yonekura Y, Ohtani H, Konishi J, Yokoyama A. (1997) Copper-62-ATSM: a new hypoxia imaging agent with high membrane permeability and low redox potential. *J Nucl Med.* **38**:1155-1160.

Hanahan D, Folkman J. (1996) Patterns and emerging mechanisms of the angiogenic switch during tumorigenesis. *Cell* **86**:353-363.

Hanahan D, Weinberg RA. (2011) Hallmarks of cancer: the next generation. *Cell* **144**(5):646-74. doi: 10.1016/j.cell.2011.02.013. Review. PubMed PMID: 21376230.

Krohn KA, Link JM, Mason RP. (2008) Molecular imaging of hypoxia. *J Nucl Med* **49**:129S-148S.

Yamaguchi S, Hirata K, Toyonaga T, Kobayashi K, Ishi Y, Motegi H, Kobayashi H, Shiga T, Tamaki N, Terasaka S, Houkin K. (2016) Change in ^{18}F-Fluoromisonidazole PET Is an Early Predictor of the Prognosis in the Patients with Recurrent High-Grade Glioma Receiving Bevacizumab Treatment. *PLoS One* **11**(12):e0167917. doi: 10.1371/journal.pone.0167917. eCollection 2016. PubMed PMID: 27936194; PubMed Central PMCID: PMC5148016.

Poster from SNMMI 2017.

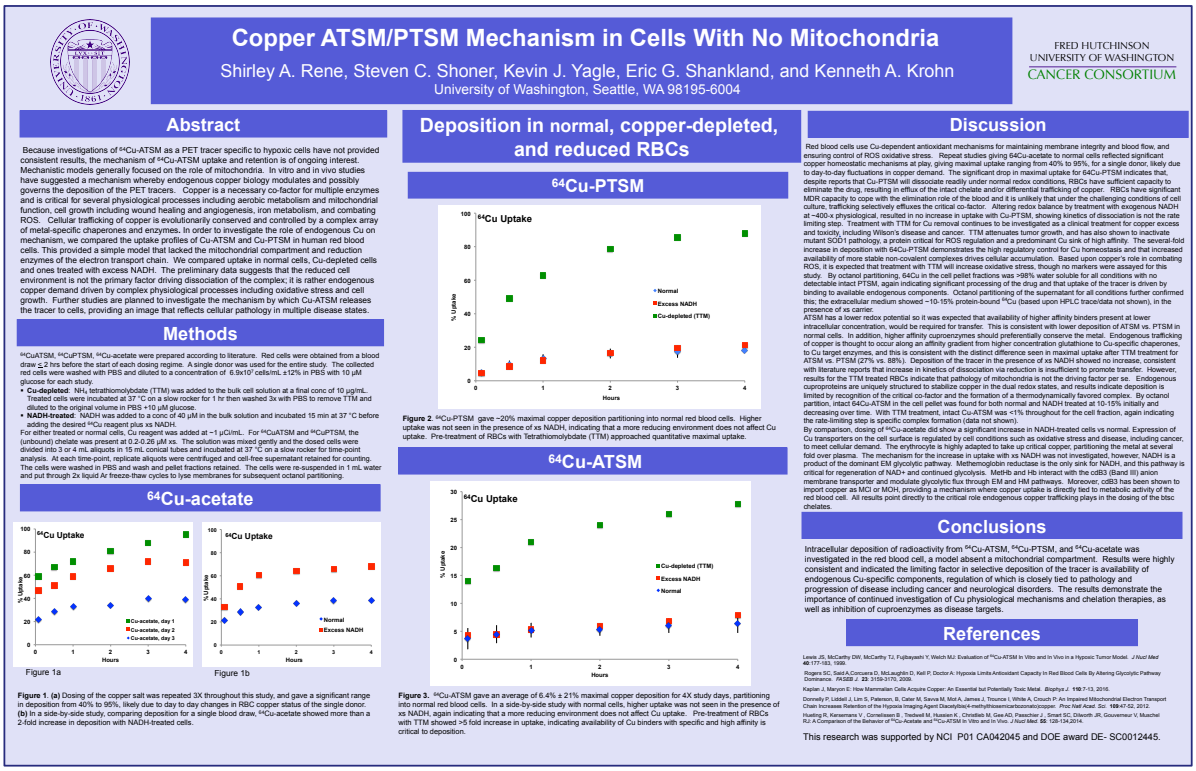

Copper ATSM/PTSM Mechanism in Cells With No Mitochondria

Shirley A. Rene, Steven C. Shoner, Kevin J. Yagle, Eric G. Shankland, and Kenneth A. Krohn
University of Washington, Seattle, WA 98195-6004

FRED HUTCHINSON UNIVERSITY OF WASHINGTON CANCER CONSORTIUM

Abstract

Because investigations of ^{64}Cu-ATSM as a PET tracer specific to hypoxic cells have not provided consistent results, the mechanism of ^{64}Cu-ATSM uptake and retention is of ongoing interest. Mechanistic models generally focused on the role of mitochondria. In vitro and in vivo studies have suggested a mechanism whereby endogenous copper biology modulates and possibly governs the deposition of the PET tracers. Copper is a necessary co-factor for multiple enzymes and is critical for several physiological processes including aerobic metabolism and mitochondrial function, cell growth including wound healing and angiogenesis, iron metabolism, and combating ROS. Cellular trafficking of copper is evolutionarily conserved and controlled by a complex array of metal-specific chaperones and enzymes. In order to investigate the role of endogenous Cu on mechanism, we compared the uptake profiles of Cu-ATSM and Cu-PTSM in human red blood cells. This provided a simple model that lacked the mitochondrial compartment and reduction enzymes of the electron transport chain. We compared uptake in normal cells, Cu-depleted cells and ones treated with excess NADH. The preliminary data suggests that the reduced cell environment is not the primary factor driving dissociation of the complex; it is rather endogenous copper demand driven by complex physiological processes including oxidative stress and cell growth. Further studies are planned to investigate the mechanism by which Cu-ATSM releases the tracer to cells, providing an image that reflects cellular pathology in multiple disease states.

Methods

^{64}CuATSM, ^{64}CuPTSM, ^{64}Cu-acetate were prepared according to literature. Red cells were obtained from a blood draw ≤ 2 hrs before the start of each dosing regime. A single donor was used for the entire study. The collected red cells were washed with PBS and diluted to a concentration of 6.9x10^{7} cells/mL ±12% in PBS with 10 µM glucose for each study.

- **Cu-depleted**: NH_4 tetrathiomolybdate (TTM) was added to the bulk cell solution at a final conc of 10 µg/mL. Treated cells were incubated at 37 °C on a slow rocker for 1 hr then washed 3x with PBS to remove TTM and diluted to the original volume in PBS +10 µM glucose.
- **NADH-treated**: NADH was added to a conc of 40 µM in the bulk solution and incubated 15 min at 37 °C before adding the desired ^{64}Cu reagent plus xs NADH.

For either treated or normal cells, Cu reagent was added at ~1 µCi/mL. For ^{64}CuATSM and ^{64}CuPTSM, the (unbound) chelate was present at 0.2-0.26 µM xs. The solution was mixed gently and the dosed cells were divided into 3 or 4 mL aliquots in 15 mL conical tubes and incubated at 37 °C on a slow rocker for time-point analysis. At each time-point, replicate aliquots were centrifuged and cell-free supernatant retained for counting. The cells were washed in PBS and wash and pellet fractions retained. The cells were re-suspended in 1 mL water and put through 2x liquid Ar freeze-thaw cycles to lyse membranes for subsequent octanol partitioning.

^{64}Cu-acetate

Figure 1a Figure 1b

Figure 1. **(a)** Dosing of the copper salt was repeated 3X throughout this study, and gave a significant range in deposition from 40% to 95%, likely due to day to day changes in RBC copper status of the single donor. **(b)** In a side-by-side study, comparing deposition for a single blood draw, ^{64}Cu-acetate showed more than a 2-fold increase in deposition with NADH-treated cells.

Deposition in normal, copper-depleted, and reduced RBCs

^{64}Cu-PTSM

Figure 2. ^{64}Cu-PTSM gave ~20% maximal copper deposition partitioning into normal red blood cells. Higher uptake was not seen in the presence of xs NADH, indicating that a more reducing environment does not affect Cu uptake. Pre-treatment of RBCs with Tetrathiomolybdate (TTM) approached quantitative maximal uptake.

^{64}Cu-ATSM

Figure 3. ^{64}Cu-ATSM gave an average of 6.4% ± 21% maximal copper deposition for 4X study days, partitioning into normal red blood cells. In a side-by-side study with normal cells, higher uptake was not seen in the presence of xs NADH, again indicating that a more reducing environment does not affect Cu uptake. Pre-treatment of RBCs with TTM showed >5 fold increase in uptake, indicating availability of Cu binders with specific and high affinity is critical to deposition.

Discussion

Red blood cells use Cu-dependent antioxidant mechanisms for maintaining membrane integrity and blood flow, and ensuring control of ROS oxidative stress. Repeat studies giving 64Cu-acetate to normal cells reflected significant copper homeostatic mechanisms at play, giving maximal uptake ranging from 40% to 95%, for a single donor, likely due to day-to-day fluctuations in copper demand. The significant drop in maximal uptake for 64Cu-PTSM indicates that, despite reports that Cu-PTSM will dissociate readily under normal redox conditions, RBCs have sufficient capacity to eliminate the drug, resulting in efflux of the intact chelate and/or differential trafficking of copper. RBCs have significant MDR capacity to cope with the elimination role of the blood and it is unlikely that under the challenging conditions of cell culture, trafficking selectively effluxes the critical co-factor. Altering redox balance by treatment with exogenous NADH at ~400-x physiological, resulted in no increase in uptake with Cu-PTSM, showing kinetics of dissociation is not the rate limiting step. Treatment with TTM for Cu removal continues to be investigated as a clinical treatment for copper excess and toxicity, including Wilson's disease and cancer. TTM attenuates tumor growth, and has also shown to inactivate mutant SOD1 pathology, a protein critical for ROS regulation and a predominant Cu sink of high affinity. The several-fold increase in deposition with 64Cu-PTSM demonstrates the high regulatory control for Cu homeostasis and that increased availability of more stable non-covalent complexes drives cellular accumulation. Based upon copper's role in combating ROS, it is expected that treatment with TTM will increase oxidative stress, though no markers were assayed for this study. By octanol partitioning, 64Cu in the cell pellet fractions was >98% water soluble for all conditions with no detectable intact PTSM, again indicating significant processing of the drug and that uptake of the tracer is driven by binding to available endogenous components. Octanol partitioning of the supernatant for all conditions further confirmed this; the extracellular medium showed ~10-15% protein-bound ^{64}Cu (based upon HPLC trace/data not shown), in the presence of xs carrier.

ATSM has a lower redox potential so it was expected that availability of higher affinity binders present at lower intracellular concentration, would be required for transfer. This is consistent with lower deposition of ATSM vs. PTSM in normal cells. In addition, higher affinity cuproenzymes should preferentially conserve the metal. Endogenous trafficking of copper is thought to occur along an affinity gradient from higher concentration glutathione to Cu-specific chaperones, to Cu target enzymes, and this is consistent with the distinct difference seen in maximal uptake after TTM treatment for ATSM vs. PTSM (27% vs. 95%). Deposition of the tracer in the presence of xs NADH showed no increase, consistent with literature reports that increase in kinetics of dissociation via reduction is insufficient to promote transfer. However, results for the TTM treated RBCs indicate that pathology of mitochondria is not the driving factor per se. Endogenous cuproproteins are uniquely structured to stabilize copper in the dual redox states, and results indicate deposition is limited by recognition of the critical co-factor and the formation of a thermodynamically favored complex. By octanol partition, intact 64Cu-ATSM in the cell pellet was found for both normal and NADH treated at 10-15% initially and decreasing over time. With TTM treatment, intact Cu-ATSM was <1% throughout for the cell fraction, again indicating the rate-limiting step is specific complex formation (data not shown).

By comparison, dosing of ^{64}Cu-acetate did show a significant increase in NADH-treated cells vs normal. Expression of Cu transporters on the cell surface is regulated by cell conditions such as oxidative stress and disease, including cancer, to meet cellular demand. The erythrocyte is highly adapted to take up critical copper, partitioning the metal at several fold over plasma. The mechanism for the increase in uptake with xs NADH was not investigated, however, NADH is a product of the dominant EM glycolytic pathway. Methemoglobin reductase is the only sink for NADH, and this pathway is critical for regeneration of NAD+ and continued glycolysis. MetHb and Hb interact with the cdB3 (Band III) anion membrane transporter and modulate glycolytic flux through EM and HM pathways. Moreover, cdB3 has been shown to import copper as MCl or MCH, providing a mechanism where copper uptake is directly tied to metabolic activity of the red blood cell. All results point directly to the critical role endogenous copper trafficking plays in the dosing of the bisc chelates.

Conclusions

Intracellular deposition of radioactivity from ^{64}Cu-ATSM, ^{64}Cu-PTSM, and ^{64}Cu-acetate was investigated in the red blood cell, a model absent a mitochondrial compartment. Results were highly consistent and indicated the limiting factor in selective deposition of the tracer is availability of endogenous Cu-specific components, regulation of which is closely tied to pathology and progression of disease including cancer and neurological disorders. The results demonstrate the importance of continued investigation of Cu physiological mechanisms and chelation therapies, as well as inhibition of cuproenzymes as disease targets.

References

Lewis JS, McCarthy DW, McCarthy TJ, Fujibayashi Y, Welch MJ. Evaluation of ^{64}Cu-ATSM In Vitro and In Vivo in a Hypoxic Tumor Model. *J Nucl Med* **40**:177-183, 1999.

Rogers SC, Said A,Corcoran D, McLaughlin D, Kell P, Doctor A. Hypoxia Limits Antioxidant Capacity in Red Blood Cells By Altering Glycolytic Pathway Dominance. *FASEB J.* **23**: 3159-3170, 2009.

Kaplan J, Maryon E. How Mammalian Cells Acquire Copper: An Essential but Potentially Toxic Metal. *Biophys J.* **110**:7-13, 2016.

Donnelly P, Liddell J, Lim S, Paterson, B, Cater M, Savva M, McLA, James J, Trounce I, White A, Crouch P. An Impaired Mitochondrial Electron Transport Chain Increases Retention of the Hypoxia Imaging Agent Diacetylbis(4-methylthiosemicarbazonato)copper. *Proc Natl Acad. Sci.* **109**:47-52, 2012.

Huang R, Karasmana V., Cornelissen B., Tredwell M, Hussien K., Christlieb M, Gee AD, Passchier J., Smart SC, Dilworth JR, Gouverneur V, Muschel RJ. A Comparison of the Behavior of ^{64}Cu-Acetate and ^{64}Cu-ATSM In Vitro and In Vivo. *J Nucl Med.* **55**: 126-134,2014.

This research was supported by NCI P01 CA042045 and DOE award DE- SC0012445.

DIAGNOSTIC APPLICATIONS OF RADIOLABELED BIOLOGICS IN SOLID TUMORS

Project 3 leader: Satoshi Minoshima, MD, PhD

The overall objective of this project is to advance imaging and future theranostic applications of biologics that are being developed in our laboratory and to conduct preclinical PET imaging of ^{89}Zr labeled anti-Glypican-3 antibody (αGPC3) in the mouse model of hepatocellular carcinoma (HCC) and liver cirrhosis and ^{89}Zr or ^{18}F labeled aptamer, Epidermal Growth Factor Receptor (EGFR) SOMAmers in animal xenograft models of EGFR overexpressing tumors. Through these projects, we will produce data that are necessary for further translational efforts to human studies and also provide training opportunities, as described separately, for physicians and basic scientists.

Biologics include a wide range of products such as tissues, cells, antibodies, peptides, genes or gene fragments, recombinant proteins. They can be produced from human and specimens, microorganisms, or biotechnologically synthesized. The developments and theranostic applications of the materials are forefront of biomedical sciences, and its feasibility and efficacies have been shown in various medical conditions including cancers. This Project is to advance diagnostic applications of such materials targeting solid tumors (HCC and brain tumor), in interdisciplinary collaboration between radiology and surgery and in consultation with radiation oncology investigators who have an extensive expertise in antibody imaging and theranostic applications.

Our laboratory has been actively working with the UW surgery faculty on the development of new radiopharmaceuticals for molecular imaging in the diagnosis of hepatocellular carcinoma (HCC). HCC is the second most lethal cancer worldwide, and it is the fifth and ninth leading cause of cancer related deaths in men and women, respectively. The US incidence of HCC is rising at epidemic proportions predominantly due to non-alcoholic fatty liver disease (NAFLD) resulting from the increasing prevalence of obesity and diabetes. NAFLD is projected to replace hepatitis C virus (HCV) infection as the leading cause of HCC in the US by 2025.

Diagnosis, staging and treatment planning of HCC has relied heavily on liver protocol computed tomography (CT) or magnetic resonance (MR) imaging. However, lack of histologic specificity limits these contrast timing-based modalities. CT/MRI detection threshold for HCC at present is a minimum of 1-2 cm tumor, consisting of over billions of cancer cells. Although overall CT/MR technology improves, and smaller tumors are detected, the ability of CT/MR to distinguish between malignant and benign entities falls short, introducing uncertainty regarding the diagnosis or disease extent. Extra---hepatic metastases neglected by these scans require additional diagnostic testing. Doubt raised by inadequate scans triggers costly repeat interval imaging, or biopsies with hemorrhage and tumor seeding risks, all contributing to delayed diagnosis and treatment [1]. An imaging platform that is more sensitive in detecting and more accurate in defining HCC will significantly improve the management and therapeutic results of HCC, while decreasing the cost of health care delivery to these patients

We have recently developed a ^{89}Zr labeled αGPC3 antibody PET imaging technology. GPC3 is a heparin sulfate proteoglycan important in regulating cell growth. It is an ideal target due to its overexpression in up to 80% of HCCs and absence in normal tissues, cirrhotic livers and benign lesions. As a membrane-bound proteoglycan, it is readily accessible to antibody-mediated targeting and immunohistochemical GPC3 staining has demonstrated 97% specificity [2]. ^{89}Zr has recently emerged as a promising PET radioisotope when conjugated with monoclonal antibodies (MAbs). Conjugation of ^{89}Zr to several pre-clinical and clinically available MAbs have demonstrated high spatial resolution and excellent signal-to-noise ratios [3]. ^{89}Zr possess an optimal half-life ($t_{1/2=}$78.4 hrs) permitting unwanted background MAb signal to clear, allowing visualization of the liver tumor [4]. We have reported the successful ^{89}Zr labeled αGPC3 PET imaging study of human HCC in a murine orthotopic xenograft model in the Journal of Nuclear Medicine [5].

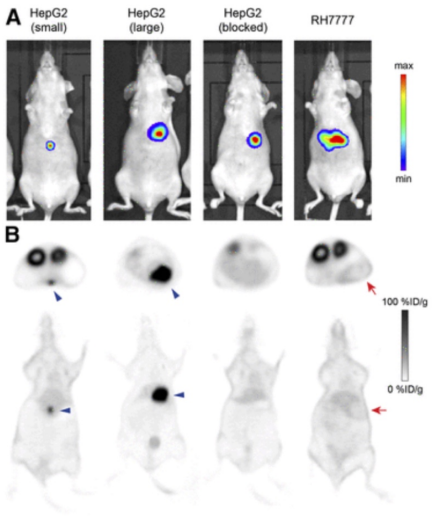

(A) Luminescent images after intraperitoneal administration of luciferin (75 mg/kg) verifying presence of intrahepatic tumor before administration of ^{89}Zr-F(ab')2. (B) Axial and coronal PET images of same animals (24 h) demonstrating tumor concordance in HepG2 animals and absence of PET signal in RH7777 tumors and blocked HepG2 controls. Blue arrowheads indicate HepG2 tumors; red arrows indicate RH7777 tumors. max = maximum; min = minimum [5]

While advancing antibody-based molecular imaging technology for possible clinical applications, another type of biologics provides a unique opportunity for radiolabeled imaging applications. The proposed project is to develop a new class of radiolabeled high affinity binding reagents, SOMAmers [6,7] as a proof of concept for molecular imaging that can bridge extensive bench-top research to translational applications to in vivo diagnostic imaging.

While the initial plan was to further investigate ^{89}Zr labeled αGPC3 antibody PET imaging and also investigate the development of radiolabeled SOMAmer targeting EGFR aptamers, with the move of the project's original PI (Dr. Satoshi Minoshima) to the University of Utah, there was a change of direction of the project. The final summary of the revised project is provided below.

Final summary report: Hepatocellular carcinoma (HCC) is the second leading cause of mortality worldwide and the most common form of liver cancer. Therapeutic options are limited with curative options including resection, ablation, or transplantation available in only a subset of patients. We initially pursued imaging with Zr-89 labeled Glypican-3–Targeting F(ab')2 in a murine model of HCC. The project was successful [5], but clinical translation could not be achieved due to the lack of availability of humanized antibodies produced in the cGMP environment. We then explored the use of tumor specific autologous T cells as a therapeutic option against HCC by replacing the natural T cell receptor (TCR) by an artificially generated tumor-specific TCR which is capable of recognizing an intracellular, tumor-specific protein in a given HLA context. Prior single center clinical studies evaluating T cells transduced with a TCR specific for NY-ESO-1, a member of the cancer-testis antigen (CTA) family, have been initiated in HLA-A2+ patients with metastasized melanoma, synovial cell sarcoma, and multiple myeloma, with an impressive overall response rate in patients with melanoma and sarcoma. CTAs may represent an ideal antigen for HCC immunotherapy and therefore are antigen targets that we are investigating. No promising adoptive transfer approaches have demonstrated efficacy for the majority of tumor types and few studies have explored using local delivery of T cells for the treatment of solid tumors in comparison to the administration of T-cells by a peripheral venous approach. To successfully explore the utilization of this therapy, the first steps involve identifying an ideal CTA target, testing the effectiveness of the TCRs in vitro, followed by in vivo assessment using radiolabeled T-cells and their in vivo distribution. We have performed immunohistochemical staining of testis and HCC tissue sections and identified the expression of CTAs NY-ESO-1, MAGE-A3, and MAGE-C1 in these samples. Further analysis of mRNA expression of HCC cell lines by reverse transcriptase PCR has determined frequent expression of all tested CTAs. The most common HLA allele in the US is HLA-A2 and development of TCR-transgenic T cells recognizing an antigen in the context of HLA-A2 should therefore enable the widest use of this therapy. We have determined the expression of HLA-A2 on multiple HCC cell lines and have identified two cell lines expressing this allele. Furthermore, we have engineered luciferase expressing HCC cell lines as well as TCR-transgenic T cells specific for the CTA NY-ESO-1 and have demonstrated that these T cells bind to the antigen and are activated by antigen-presenting cells

loaded with the cognate NY-ESO-1 peptide. We have completed testing of the NY-ESO-1 specific T cells against the HCC cell line HepG2 by determining luciferase activity after co-culture of T cells and target cells at different effector-target ratios and have demonstrating effective killing with the NY-ESO-1 specific T cells. Additionally, we have implanted human HepG2 xenografts in NOD-SCID mice and are currently in the process of evaluating the efficacy of our treatments in vivo. Once we have shown via in vivo optical imaging system (IVIS) that our therapy is effective, we will assess efficacy of local delivery of therapy versus systemic (peripheral IV). T cells will be radiolabeled T cells and administered via local delivery vs peripheral IV. Target uptake and biodistribution will be assessed, and efficacy of image-guided local delivery of TCRs will be compared.

References:

[1]. Silva, M.A., et al., *Needle track seeding following biopsy of liver lesions in the diagnosis of hepatocellular cancer: a systematic review and meta-analysis.* Gut, 2008. 57(11):p. 1592-6.

[2]. Capurro, M.,et al.,*Glypican-3:a novel serum and histochemical marker for hepatocellular carcinoma.* Gastroenterology, 2003. 125(1): p. 89-97.

[3]. Zhang, Y., H. Hong, and W. Cai, *PET tracers based on Zirconium-89.* Curr Radiopharm, 2011. 4(2): p. 131-9.

[4]. Wright,B.D. and S.E. Lapi, *Designing the magic bullet? The advancement of immuno-PET into clinical use.* J Nucl Med, 2013. 54(8): p. 1171-4.

[5]. Sham, J.G., et al., *Glypican-3-Targeted 89Zr PET Imaging Of Hepatocellular Carcinoma.* J Nucl Med, 2014;55:2032-2037

[6]. Gold, L., et al., *Aptamer-based Multiplexed proteomic technology for biomarker discovery.* PLoS One, 2010. 5(12): p. e15004.

[7]. Ostroff, R.M., et al., *Unlocking biomarker discovery: large scale application of aptamer proteomic technology for early detection of lung cancer.* PLoS One, 2010. 5(12):p.e15003.